THE LUMINESCENT PROPERTIES OF EUROPIUM THENOYLTRIFLOUROACETONE CCOMPLEXES WITH 2-PHENYL-1H-IMIDAZO[4,5-f][1,10]PHENANTHROLINE BASED LIGANDS.

A thesis presented to the faculty of the Graduate School of Western Carolina University in partial fulfillment of the requirements for the degree of Master of Science in Chemistry.

By

Paul Jacob Venturo

Director: Dr. Brian Dinkelmeyer
Associate Professor of Chemistry
Department of Chemistry and Physics

Committee Members: Dr. Channa De Silva, Dr. William Kwochka

October 2020

ACKNOWLEDGEMENTS

My acknowledgements go out to my family for their constant support, my friends who kept me going for all these year, Dr. Dinkelmeyer and Dr. De Silva for all their insight and advice along with helping to answer my many questions, and finally to the rest of the faculty and staff within the Department of Chemistry and Physics. Without all of you this could never be a possibility.

TABLE OF CONTENTS

LIST OF FIGURES

LIST OF TABLES

List of Abbreviations

UV	Ultraviolet
UV-Vis	Ultraviolet-visible
NMR	Nuclear Magnetic Resonance
HNMR	Proton NMR
CNMR	Carbon NMR
IR	Infrared
FT-IR	Fourier-Transform Infrared
DFT	Density Functional Theory
TDDFT	Time Dependent Density Functional Theory
DCM	Dichloromethane
DMSO	Dimethyl sulfoxide
TTA	Thenoyltrifluoroacetone
PIP	Phenyl-1H-imidazo[4,5-f][1,10]phenanthroline
PIP-2tolu	2-Tolu-1H-imidazo[4,5-f][1,10]phenanthroline
PIP-4tolu	4-Tolu-1H-imidazo[4,5-f][1,10]phenanthroline
PIP-2CF_3	[2-triflouromethy-phenyl]-1H-imidazo[4,5-f][1,10]phenanthroline
PIP-4CF_3	[4-triflouromethy-phenyl]-1H-imidazo[4,5-f][1,10]phenanthroline
PIP-2nitro	[2-nitro-phenyl]-1H-imidazo[4,5-f][1,10]phenanthroline
PIP-4nitro	[4-nitro-phenyl]-1H-imidazo[4,5-f][1,10]phenanthroline

ABSTRACT

THE LUMINESCENT PROPERTIES OF EUROPIUM THENOYLTRIFLOUROACETONE CCOMPLEXES WITH 2-PHENYL-1H-IMIDAZO[4,5-f][1,10]PHENANTHROLINE BASED LIGANDS.

Paul Venturo, M.S

Western Carolina University (October 2020)

Director: Dr. Brian Dinkelmeyer

The goal of this work is to synthesize a series of europium complexes based on 2-phenyl-1H-imidazo[4,5-f][1,10]phenanthroline ligand structure and optimize the luminescent quantum yield and fluorescence of lanthanide complexes and to gain an understanding of how the structure of the coordinating ligand influences the lanthanide luminescence. Lanthanide complexes have gone through some interesting developments in the past few years and the applications of these complexes continue to expand. The applications of their luminescent and spectroscopic properties can be found in fields such as chemistry, optics, engineering, and biomedical imaging. Many of these properties are caused by the unique electron configuration of the lanthanide ions. The purpose of this research is to observe and measure the fluorescent properties of europium complexes containing 2-phenyl-1H-imidazo[4,5-f][1,10]phenanthroline (PIP) based ligands. In this project, the PIP ligands are first synthesized then reacted with $Eu(TTA)_3$ $(H_2O)_2$ to form europium PIP complexes. The ligands were characterized using FT-IR, ^{1}H NMR, ^{13}C NMR, UV-

Vis, and Fluorescence spectroscopy. The luminescent quantum yields of the complexes were calculated using $Eu(TTA)_3(H_2O)_2$ as the standard. Density functional theory (DFT) calculations were carried out throughout the process to evaluate the structural and spectroscopic properties of both the ligands and their respected complexes. From the results, the only trend that was observed was between the ΔE_{ISC} and the luminescent quantum yield where a ΔE_{ISC} between 0.73-0.76 eV gave higher quantum yield values.

CHAPTER 1: INTRODUCTION

1.1 Project Goal

The goal of this research is to observe and quantify the fluorescence of lanthanide complexes and to obtain a further understanding of how the structure of the coordinated ligand influences the luminescence. A family of 2-phenyl-1H-imidazo[4,5-f][1,10]phenanthroline ligands were synthesized which contained either electron-donating or electron-withdrawing substituents groups in the ortho or para phenyl positions. The nature and position of these groups should affect the quantum efficiency of their Eu^{3+} complexes. Studying these similar Eu^{3+} complexes and their luminescent properties should provide insight into structure-property relationships influencing the quantum yield of these complexes. The possible correlations found in this project could open the door to more possible uses for these kinds of europium complexes through minor augmentations of the ligand. With the many properties that Eu^{3+} complexes have, such as long luminescent lifetimes and large stokes shifts, these products could see more use in applications such as bio labelling and laser confocal scanning microscopy. This was all done by synthesizing and chelating both the ligands and the final complexes as well as using computational analysis through density functional theory to ascertain possible trends by comparing the theoretical data with the experimental luminescent quantum yields.

1.2 Background

Lanthanide complexes have gone through some interesting developments in the past few years. When the common europium (III) is chelated with appropriate organic ligands the product complexes have been known to have a long luminescent lifetime and a narrow emission band

emitting red light at approximately 615 nm when excited with UV light. With many of these ligands it is observed the wavelength of the emission band is constant though the emission intensity is affected by changing the ligand structures. In addition to having high stokes shifts and long luminescent lifetimes, these Eu^{3+} complexes often have high luminescent quantum yields.[1] It is these properties (long luminescent lifetimes, large Stokes shift, and high quantum yield) that make Eu^{3+} complexes interesting and ripe for development into devices and diagnostic tools. Some applications for these lanthanide complexes, in particular europium, include dopants for organic light emitting diodes, bio labeling, and as fluorescent dyes for confocal microscopy.[2]

This fixed emission wavelength of Eu^{3+} complexes is due to having negligible f orbital interactions with the ligand orbitals. The minimum ligand field effects are due the shielding of *f*-orbitals by the filled 5*s* and 5*p* subshells. Figure 1 shows the ligand to metal energy transfer process in a n europium complex resulting in an europium-centered emission.

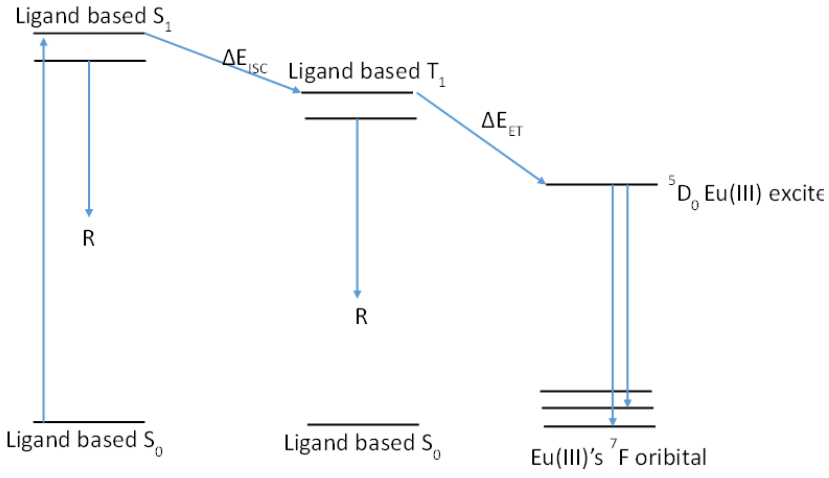

Figure 1. Electronic Energy transfer processes in lanthanide complexes

When electrons on the ligand are excited from π to π*, they then undergo intersystem crossing to form a triplet state. Relaxation of the triplet state results in energy transfer into the $^5D_1$ or $^5D_0$ europium excited states.[3] The transferred energy assists in the population of the europium's excited states and the later emission is caused by the radiative relaxation of those excited electrons. However, in order for the electron to move into the resonance level of $^5D_0$ of the Eu(III) the lowest triplet state of the complex must have an energy relatively close to 2.14493 eV, this being the energy of the $^5D_0$ orbital of Eu.[4,5] The emissions produced from the radiative relaxations from these europium excited states is what is referred to as lanthanide-centered luminescence. The earlier mentioned lowest triplet states have also been found to have correlations to the luminescent quantum yield of these Eu^{3+} complexes.[6] More specifically it has been found that variations in the energy of the energy transfer (ΔE_{ET}) and intersystem crossing (ΔE_{ISC}) have been correlated to the quantum yield of lanthanide complexes as a whole.[7] The equation for both ΔE_{ET} and ΔE_{ISC} can be found in the equations below in equations 1 and 2.

$$Lowest\ Singlet\ E(eV) - Lowest\ Triplet\ E\ (eV) = \Delta E_{ISC} \quad (1)$$

$$Lowest\ Triplet\ E(eV) - 2.14493(eV) = \Delta E_{ET} \quad (2)$$

The quantum yield is the ratio of the number of photons emitted compared the number of photons absorbed by the complex.[8]

$$\Phi = \frac{\#\ photons\ emitted}{\#\ photons\ absorbed} \quad (3)$$

This would mean that a complex or chemical with a quantum yield of 1 or 100% emits 100% of the light that has been absorbed. As it is not possible to record quantum yield directly, a relative quantum yield can be calculated instead.

Because of its intrinsic luminescent properties and ultraviolet reactivity, europium has been one of the primary lanthanides being looked at for a variety of purposes. As lanthanides have been observed to produce narrow emission bands, europium which emits at approximately 615 nm, is being used as a possible chromophore for red light.[9] With europium's strong and specific red emission, it has been looked at for monochromatic LEDs, removing the need for a filter to cut out the undesired wavelengths produced by broad emissions of organic molecules.[10] While some research has continued looking at europium as an emitter, others have been looking into uses for its ultraviolet reactivity for uses like a UV detection method or in the use of solar panels.[11] One of these suggests the use of europium complexes as UV conversion layer, as many of the current solar cells have minimal responsiveness to short-wavelength photons. Using these complexes allows for the easy conversion of UV light to visible light resulting in greater efficiency of energy generation.[12] The ligands that much of the current research has been interested in have been both β-diketones as they have been known to transfer energy to the lanthanides and neutral bidentate ancillary ligands such as bipyridine and phenanthroline groups which both increase the luminescence and stability of the complex.[13]

For computational experiments on europium complexes, the most popular level of theory has been density functional theory (DFT) and with much of these investigating the excited states of these complexes, time dependent density functional theory (TDDFT) has become the preferred method.[4] For the basis sets in use for the Eu^{3+} metal center, Stuttgart/Dresden based effective core potential (ECP) basis sets, while for the ligands most have been using either 6-31G or 6-311G.[4,14,15]

For all of the theoretical work that were involved in the project, density functional theory (DFT) calculations were used. DFT calculations are much like semiempirical calculations, such

as Hartree-Fock approximation, are based on the Schrodinger equation. Unlike Hartree-Fock, DFT does not calculate a wavefunction but instead calculates the electron density function.[16] One advantage of using DFT over Hartree-Fock is that the calculations are more cost effective and it is able to do so by making more approximations through the use of functionals such as BLYP and B3LYP.[17] Another useful function to DFT that was in use in this project was its ability to have a time dependent function to the calculations. Time dependent density functional theory (TDDFT) can be used to calculate the luminescent and spectral data of a given structure by describing the electronic excited states, all of this being possible by adding that time dependent function to DFT.

1.3 Project Design

The primary goal for this project was to synthesize and observe the luminescent properties of europium complexes with molecular variations of 2-phenyl-1H-imidazo[4,5-f][1,10]phenanthroline ligand (PIP) and testing them against theoretical calculations made through computational methods. The synthesis of the ligand and complex are outlined in Figure 2. The first step was converting 1,10-phenathroline (1) to 1,10-phenanthroline-5,6-dione (2) through a reaction using potassium bromide, concentrated sulfuric acid, and fuming nitric acid. The resulting 1,10-phenanthroline-5,6-dione is then reacted with a benzaldehyde constituent and ammonium acetate in glacial acetic acid to produce a of 2-phenyl-1H-imidazo[4,5-f][1,10]phenanthroline ligand (3). The final europium complex (4) can finally be synthesized using a 1:1 ratio of ligand (3) and $Eu(TTA)_3$ $(H_2O)_2$ in 10 mL of methanol. The quantum yield is then quantified for the europium complex and the results were compared with the theoretical data obtained through computational analysis.

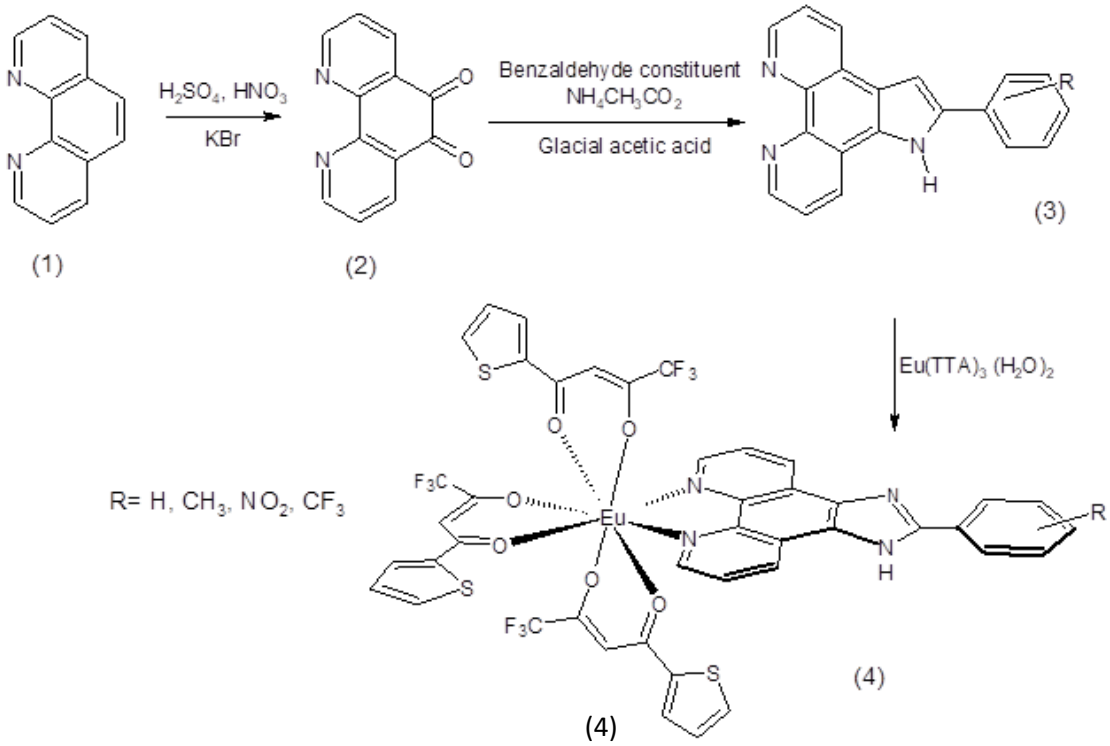

Figure 2. Complete reaction scheme for the project

As for the computational calculations, all calculations were done using Gaussian 09 computational chemistry software. Geometric optimizations were done using DFT level of theory with the B3LYP hybrid exchange correlation function. For C, N, O, F, and H, a 6-31G* basis set was used whereas for the europium ion, MWB52 was used. Absorption properties and electronic excited states were calculated using TDDFT level of theory.

Chapter 2 EXPERIMENTAL

All reagents were purchased from Sigma Aldrich, Fisher Science, and Acros Organics, and were used without further purification unless otherwise stated. Synthesized ligands were characterized using Fourier-transform infrared spectroscopy (FT-IR), nuclear magnetic

resonance (NMR, when applicable), UV-visible and fluorescence spectroscopic techniques. The methods used for characterization will be discussed in this section along with all instrument specifications.

2.1 FT-IR

FT-IR spectra were obtained using a Perkin Elmer Spectrum One. All measurements were performed at room temperature with a scanning range of 4000 cm^{-1} – 600 cm^{-1}, using single-bounce attenuated total reflectance with a diamond crystal. For all of the materials that were measured as a solid powder (all solvents had been removed), the background was performed on the instrument in a room temperature environment. The ATR plate was cleaned with a Kimwipe and acetone between each measurement.

2.2 Nuclear Magnetic Resonance Spectroscopy (NMR)

NMR spectra were obtained using a JEOL 300 MHz Eclipse NMR with a 5 mm probe capable of detecting ^{1}H and ^{13}C nuclei. Proton NMR samples were prepared using ~10 mg of material, in either deuterated chloroform ($CDCl_3$) or deuterated dimethyl sulfoxide (d6-DMSO) unless otherwise stated, and spectra were obtained using a varying number of scans ranging from 16-128 as to ensure an adequate signal-to-noise ratio was acquired. ^{13}C NMR samples were prepared similarly, except material was added until the deuterated solution became saturated.

2.3 UV-Visible Absorption Spectroscopy

UV-Vis spectra were collected using an Agilent Cary 5000 UV-vis-NIR spectrometer at room temperature. This instrument has two different sources: a deuterium lamp (for UV measurements), and a tungsten lamp (for visible measurements). The use of a photodiode array detector allows the spectrometer to detect a wavelength range of 190 nm – 1100 nm at 1 nm

intervals. All of the blank and sample measurements were made using a quartz cuvette (1 cm path length). The solvent used for each experiment was dichloromethane. For the quantum yield measurements, $Eu(TTA)_3(H_2O)_2$ was used as a reference and was treated the same as the samples. All samples used for the quantum yield experiment would have their concentrations adjusted so that the absorbance value at 340 nm was at between 0.3-0.4. Each sample was then measured in triplicate for three days.

2.4 Fluorescence Spectroscopy

Fluorescence spectra were acquired using a Perkin Elmer LS-55 Luminescence Spectrometer at room temperature. The same solvent systems for the blanks (to correct for any solvent fluorescence), samples and references that were used for UV-Vis measurements were also used for fluorescence measurements. A quartz cuvette was used for all measurements. A 14 scanning range of 200 nm – 800 nm with a scan speed of 200 nm/min was used, with an excitation and emission slit of 5.0 nm.

Quantum Yield Measurements

The quantum yield calculations were calculated on Microsoft Excel using the equation:

$$\Phi = \Phi_{ref} \frac{A_{ref} I_s \eta_s^2}{A_s I_{ref} \eta_{ref}^2}$$

where Φ_{ref} is the quantum yield of the known standard, A_{ref} and A_s are the absorption measurements of the reference and sample, I_{ref} and I_s are the integrated emission area of the reference and sample, and η_{ref} and η_s are the refractive index of the reference and sample solvent. $Eu(TTA)_{3(}H_2O)_2$ (Φ=0.21) was chosen as the reference compound because the quantum yield of the complex is consistent and well-studied. For both the reference and sample, dichloromethane(n=1.4244) was as the solvent. Both the sample and the reference would have

the same excitation wavelength at 340 nm and the emission range used for the integrated fluorescence intensity was from 500-750 nm. Each sample and reference were measured in triplicate for three separate days. The excitation band of 340nm was selected since it corresponds to the absorption wavelength of TTA and gave the highest luminescent intensity.

2.5 Computational Analysis

All calculations were performed using Gaussian 09 computational chemistry software package. Geometric optimizations were carried out-using density functional theory (DFT) with the B3LYP hybrid exchange correlation function. For C, N, O, F, and H, a 6-31G* basis set was employed whereas for the europium ion, the energy-consistent relativistic effective core potentials (large-core RECPs) developed by the Stuttgart group were used with the optimized valence basis sets supplemented by polarization functions. Absorption properties and vertical excitation energies at the optimized ground-state geometries were calculated using time dependent density functional theory (TDDFT)

2.6 Synthesis of 1,10-phenanthroline-5,6-dione

1,10-phenantroline (2.0116g, 11.16 mmol, 1 eqv) was weighed into a 100 mL round bottom flask along with potassium bromide (2.0886g, 17.45 mmol, 1.56 eqv). After setting up a condensing column, slowly add cooled concentrated sulfuric acid (20mL, 33.43eqv). An orange bromine gas should form as the sulfuric acid is added and this was continually purged with argon. Stir the solution and add the fuming nitric acid (10mL, 21.46 eqv) drip by drip. Once all the nitric acid had been added, the solution was heated to reflux and stir overnight. The next day the solution was poured over ice in a 250 mL or 500 mL beaker and slowly neutralize the acid

using 125 mL of 6M sodium hydroxide or until the pH was between 6 and 7. If there was a solid orange precipitate gather this using a vacuum filter before extracting with dichloromethane and dried with magnesium sulfate. After extraction, dry using magnesium sulfate and evaporate under vacuum pressure. Yield: 1.8301 (78%)

2.7 Phenyl-1H-imidazo[4,5-f][1,10]phenanthroline (PIP)[18]

1,10-phenanthroline-5,6-dione (0.3012g ,1.433 mmol, 1 eqv) was weighed out along with ammonium acetate(2.2032g, 28.660 mmol, 20 eqv) and benzaldehyde (0.172 mL, 1.720 mmol, 1.2 eqv). To this, approximately 5 mL of glacial acetic acid was added to the round bottom flask and the mixture was allowed to reflux for 3 hours. After the refluxing period was complete, the mixture was allowed to cool and dilute with water. The acetic acid was neutralized using approximately 5 mL of concentrated ammonia hydroxide in which a precipitate will form or until neutral. The precipitate was collected by vacuum filtration. Yield: 0.3752 g (80.23%). ^{1}H-NMR (d_6-DMSO, 300MHz): δ 9.001 (dd, 2H), 8.903 (dd, 2H), 8.276 (d, 2H), 7.801 (q, 2H), 7.601 (t, 2H), 7.531 (t, 1H)^{13}C NMR 300 MHz: (d_6-DMSO, 300MHz): δ 150.1, 148.3, 144.1, 130.5, 130.1, 129.5, 126.7, 123.8. FTIR (ATR): 3063, 1460, 1352, 1072, 800.27, 736.94 cm^{-1}. UV/vis (MeOH): λmax = 274 nm, 288 nm, 226 nm, 234 nm, 325 nm.

2.8 2-Tolu-1H-imidazo[4,5-f][1,10]phenanthroline (PIP-2tolu)

1,10-phenanthroline-5,6-dione (0.2046g ,1.433 mmol, 1 eqv) was weighed out along with ammonium acetate(2.2032g, 28.660 mmol, 20 eqv) and 2-tolualdehyde (0.135 mL, 1.168 mmol, 1.2 eqv). To this, approximately 5 mL of glacial acetic acid was added to the round bottom flask and the mixture was allowed to reflux for 3 hours. After the refluxing period was complete, the mixture was allowed to cool and dilute with water. The acetic acid was then was then neutralized

using approximately 5 mL of concentrated ammonia hydroxide in which a precipitate will form or until neutral. The precipitate was collected by vacuum filtration. Yield: 01882 (62.30%). ^{1}H-NMR (d_6-DMSO, 300MHz): δ 9.026 (dd, 2H), 8.924 (dd, 2H), 8.290 (d, 2H), 7.827 (q, 2H), 7.609 (t, 2H), 7.536 (t, 1H)^{13}C NMR 300 MHz: (d_6-DMSO, 300MHz): δ =151.6, 148.3, 143.9, 137.7, 137.6, 132.0, 131.9, 130.4, 130.3, 130.0, 129.9, 126.6, 123.9, 21.6. . FTIR (ATR): 3120.18, 1607, 1483, 1351, 1188, 1124, 735 cm^{-1}. UV/vis (MeOH): λmax = 274 nm, 288 nm, 224 nm.

2.9 4-Tolu-1H-imidazo[4,5-f][1,10]phenanthroline (PIP-4tolu)

1,10-phenanthroline-5,6-dione (0.2046g ,1.433 mmol, 1 eqv) was weighed out along with ammonium acetate(2.2032g, 28.660 mmol, 20 eqv) and 4-tolualdehyde (0.135 mL, 1.168 mmol, 1.2 eqv). To this, approximately 5 mL of glacial acetic acid was added to the round bottom flask and the mixture was allowed to reflux for 3 hours. After the refluxing period was complete, the mixture was allowed to cool and dilute with water. The acetic acid was then was then neutralized using approximately 5 mL of concentrated ammonia hydroxide in which a precipitate will form or until neutral. The precipitate was collected by vacuum filtration. Yield: 0.2623 (87.99%). ^{1}H-NMR (d_6-DMSO, 300MHz): δ 9.023 (dd, 2H), 8.917 (d, 2H), 7.825 (m, 3H), 7.439 (s, 3H), 2.396 (s, 3H). ^{13}C NMR 300 MHz: (d_6-DMSO, 300MHz): δ 151.3, 148.3, 144.1, 139.9, 130.2, 127.8, 126.7, 123.84, 21.6. FTIR (ATR): 3052, 1604, 1662, 1779, 1396, 1350, 1187, 1069, 802, 736 cm^{-1}. UV/vis (MeOH): λmax = 265 nm, 286 nm, 238 nm, 212 nm.

2.10 [2-triflouromethy-phenyl]-1H-imidazo[4,5-f][1,10]phenanthroline (PIP-2CF$_3$)

1,10-phenanthroline-5,6-dione (0.2051g ,0.9758 mmol, 1 eqv) was weighed out along with ammonium acetate(1.5043 g, 19.5157 mmol, 20 eqv) and 2-(trifluoromethyl)benzaldehyde

(0.154 mL, 1.1709 mmol, 1.2 eqv). To this, approximately 5 mL of glacial acetic acid was added to the round bottom flask and the mixture was allowed to reflux for 3 hours. After the refluxing period was complete, the mixture was allowed to cool and dilute with water. The acetic acid was then was then neutralized using approximately 5 mL of concentrated ammonia hydroxide in which a precipitate will form or until neutral. The precipitate was collected by vacuum filtration. Yield: 0.1882 (52.94%). ^{1}H-NMR (d_6-DMSO, 300MHz): δ 9.026 (dd, 2H), 8.924 (dd, 2H), 8.290 (d, 2H), 7.827 (q, 2H), 7.609 (t, 2H), 7.536 (t, 1H)^{13}C NMR 300 MHz: (d_6-DMSO, 300MHz): δ =151.6, 148.3, 143.9, 137.7, 137.6, 132.0, 131.9, 130.4, 130.3, 130.0, 129.9, 126.6, 123.9, 21.6FTIR (ATR): 3062, 1605, 1565, 1442, 1310, 1175, 1122, 1132, 954, 807, 740 cm^{-1}. UV/vis (MeOH): λmax = 242 nm, 250 nm, 284 nm, 212 nm.

2.11 [4-triflouromethy-phenyl]-1H-imidazo[4,5-f][1,10]phenanthroline (PIP-4CF$_3$)

1,10-phenanthroline-5,6-dione (0.2274 g , 1.082 mmol, 1 eqv) was weighed out along with ammonium acetate(1.6679 g, 21.6376 mmol, 20 eqv) and 4-(trifluoromethyl)benzaldehyde (1.2982 mmol, 1.2 eqv). To this, approximately 5 mL of glacial acetic acid was added to the round bottom flask and the mixture was allowed to reflux for 3 hours. After the refluxing period was complete, the mixture was allowed to cool and dilute with water. The acetic acid was then was then neutralized using approximately 5 mL of concentrated ammonia hydroxide in which a precipitate will form or until neutral. The precipitate was collected by vacuum filtration. Yield: 0.1511 (38.33%). ^{1}H-NMR (d_6-DMSO, 300MHz): δ 9.050 (s, 2H), 8.843 (q, 2H), 7.948 (m,7H). ^{13}C NMR 300 MHz: (d_6-DMSO, 300MHz): δ 148.8 148.6, 148.5, 144.2, 135.9, 133.1, 132.9, 130.4, 130.1, 128.8, 128.4, 127.3, 126.6, 126.1, 124.4, 124.1, 123.9, 122.5, 119.8. FTIR (ATR): 3067, 1607, 1321, 1182, 1131, 1065, 804, 739 cm^{-1}. UV/vis (MeOH): λmax = 276 nm, 223 nm, 287 nm.

2.12 [2-nitro-phenyl]-1H-imidazo[4,5-f][1,10]phenanthroline (PIP,2nitro)

1,10-phenanthroline-5,6-dione (0.9520 mmol, 1 eqv) was weighed out along with ammonium acetate(1.4678 g, 19.0418mmol, 20 eqv) and 2-nitrobenzaldehyde (0.1727, 1.1425 mmol, 1.2 eqv). To this, approximately 5 mL of glacial acetic acid was added to the round bottom flask and the mixture was allowed to reflux for 3 hours. After the refluxing period was complete, the mixture was allowed to cool and dilute with water. The acetic acid was then was then neutralized using approximately 5 mL of concentrated ammonia hydroxide in which a precipitate will form or until neutral. The precipitate was collected by vacuum filtration. Yield: 0.1953 (62.85%). ^{1}H-NMR (d_6-DMSO, 300MHz): δ 9.041 (d, 2H), 8.794 (d, 2H), 8.089 (2, 2H), 7.924 (t, 1H), 7.818 (m, 3H). ^{13}C NMR 300 MHz: (d_6-DMSO, 300MHz): δ 149.3, 148.7, 146.9, 144.2, 133.4, 131.6, 131.4, 130.2, 125.0, 124.6, 124.0. FTIR (ATR): 3061, 1608, 1533, 1450, 1363, 1124, 955, 851, 809, 738, 718 cm^{-1}. UV/vis (MeOH): λmax = 257 nm, 249 nm, 282 nm, 213 nm.

2.13 [4-nitro-phenyl]-1H-imidazo[4,5-f][1,10]phenanthroline (PIP-4nitro)

1,10-phenanthroline-5,6-dione (0.2017 g , 0.9596 mmol, 1 eqv) was weighed out along with ammonium acetate(1.4794 g, 19.1921mmol, 20 eqv) and 4-nitrobenzaldehyde (0.1740 g, 1.1515 mmol, 1.2 eqv). To this, approximately 5 mL of glacial acetic acid was added to the round bottom flask and the mixture was allowed to reflux for 3 hours. After the refluxing period was complete, the mixture was allowed to cool and dilute with water. The acetic acid was then was then neutralized using approximately 5 mL of concentrated ammonia hydroxide in which a precipitate will form or until neutral. The precipitate was collected by vacuum filtration. Yield: 0.1608 (49.09%).^{1}H-NMR (d_6-DMSO, 300MHz): δ 9.011 (dd, 2H), 8.872 (d, 2H), 8.474 (m, 4H), 7.813 (q, 2H)^{13}C NMR 300 MHz: (d_6-DMSO, 300MHz): δ 148.9, 148.7, 147.9, 134.4,

130.3, 127.5, 124.9, 123.9. FTIR (ATR): 3078, 1600, 1508, 1340, 1107, 955, 855, 737, 705 cm^{-1}. UV/vis (MeOH): λmax = 257 nm, 234 nm, 287 nm, 369 nm.

2.14 Synthesis of $Eu(TTA)_3(H_2O)_2$ [19]

Europium(III) chloride hexahydrate (0.1832g, 0.5 mmol, 1 eqv) was first dissolved in 4.8 mL of water in a 25 mL round bottom flask. At the same time, sodium hydroxide (0.0510g, 1.5 mmol, 3 eqv) was dissolved in approximately 9 mL of water. To the sodium hydroxide solution, TTA (0.3333 g, 1.5 mmol, 3 eqv) was added and was then stirred at room temperature for 10 minutes. Once the sodium hydroxide and TTA mixture was completely dissolved, it was added dropwise into the europium chloride solution. After the TTA solution was added, stir the solution at 60°C for 3 hours. After the 3 hours have elapsed, remove the white precipitate through vacuum filtration and wash with 500 mL of cold water. Yield: 0.7846 g (83%).[20] UV/vis (DCM): λmax = 275 nm, 340 nm. Fluorescence (DCM, λex=340) : λem = 615 nm, 594 nm, 580 nm, 676 nm, 540 nm.

2.15 Synthesis of $Eu(TTA)_3PIP$ [20]

PIP (0.01298 g, 0.0438 mmol, in 5 mL methanol) and $Eu(TTA)_3(H_2O)_2$ (0.03729 g, 0.04379 mmol, in 5 mL of methanol) were first mixed together in a 25-50 mL Erlenmeyer flask. The resulting solution was then allowed to stir at 50°C for 30 minutes. Then a septum or cork was placed onto the Erlenmeyer bottom flask and the solution was allowed to stir at room temperature overnight. The solution was then filtered and was allowed to evaporate at room temperature leaving a crystalline product. UV/vis (DCM): λmax = 340 nm, 301 nm, 282 nm. Fluorescence (DCM, λex=340) : λem = 615 nm, 594 nm, 580 nm, 676 nm, 540 nm. Fluorescence quantum yield (λex= 340 nm, reference: $Eu(TTA)_3(H_2O)_2$ in dcm with Φ = 0.21): 46.15±3.0%.

2.16 Synthesis of $Eu(TTA)_3PIP$-2tolu

PIP-2tolu (0.01104 g, 0.03558 mmol, in 5 mL methanol) and $Eu(TTA)_3(H_2O)_2$ (0.03030 g, 0.03558 mmol, in 5 mL methanol) were first mixed together in a 25-50 mL Erlenmeyer flask. The resulting solution was then allowed to stir at 50°C for 30 minutes. Then a septum or cork was placed onto the Erlenmeyer bottom flask and the solution was allowed to stir at room temperature overnight. The solution was then filtered and was allowed to evaporate at room temperature leaving a crystalline product. UV/vis (DCM): λmax = 340 nm, 304 nm, 284 nm. Fluorescence (DCM, λex=340) : λem = 615 nm, 594 nm, 580 nm, 676 nm, 540 nm. Fluorescence quantum yield (λex= 340 nm, reference: $Eu(TTA)_3(H_2O)_2$ in dcm with Φ = 0.21): 61.78±7.5%.

2.17 Synthesis of $Eu(TTA)_3PIP$-4tolu

PIP-4tolu (0.01104 g, 0.03558 mmol, in 5 mL methanol) and $Eu(TTA)_3(H_2O)_2$ (0.03030 g, 0.03558 mmol, in 5 mL methanol) were first mixed together in a 25-50 mL Erlenmeyer flask. The resulting solution was then allowed to stir at 50°C for 30 minutes. Then a septum or cork was placed onto the Erlenmeyer bottom flask and the solution was allowed to stir at room temperature overnight. The solution was then filtered and was allowed to evaporate at room temperature leaving a crystalline product. UV/vis (DCM): λmax = 343 nm, 290 nm, 277 nm. Fluorescence (DCM, λex=340) : λem = 615 nm, 594 nm, 580 nm, 676 nm, 540 nm. Fluorescence quantum yield (λex= 340 nm, reference: $Eu(TTA)_3(H_2O)_2$ in dcm with Φ = 0.21): 60.80±7.4%.

2.18 Synthesis of $Eu(TTA)_3PIP$-$2CF_3$

PIP-$2CF_3$ (0.01298 g, 0.03563 mmol, in 5 mL methanol) and $Eu(TTA)_3(H_2O)_2$ (0.03034 g, 0.03563 mmol, in 5 mL methanol) were first mixed together in a 25-50 mL Erlenmeyer flask. The resulting solution was then allowed to stir at 50°C for 30 minutes. Then a septum or cork

was placed onto the Erlenmeyer bottom flask and the solution was allowed to stir at room temperature overnight. The solution was then filtered and was allowed to evaporate at room temperature leaving a crystalline product. UV/vis (DCM): λmax = 340 nm, 290 nm, 270 nm. Fluorescence (DCM, λex=340) : λem = = 615 nm, 594 nm, 580 nm, 676 nm, 540 nm. Fluorescence quantum yield (λex= 340 nm, reference: $Eu(TTA)_3(H_2O)_2$ in dcm with Φ = 0.21): 60.03±8.5%.

2.19 Synthesis of $Eu(TTA)_3$PIP-4CF_3

PIP-4CF_3 (0.01328 g, 0.03646 mmol, in 5 mL methanol) and Eu(TTA)3(H2O)2 (0.03105 g, 0.03646 mmol, in 5 mL methanol) were first mixed together in a 25-50 mL Erlenmeyer flask. The resulting solution was then allowed to stir at 50^{o}C for 30 minutes. Then a septum or cork was placed onto the Erlenmeyer bottom flask and the solution was allowed to stir at room temperature overnight. The solution was then filtered and was allowed to evaporate at room temperature leaving a crystalline product. UV/vis (DCM): λmax =340 nm 284 nm, 301 nm. Fluorescence (DCM, λex=340) : λem = = 615 nm, 594 nm, 580 nm, 676 nm, 540 nm. Fluorescence quantum yield (λex= 340 nm, reference: $Eu(TTA)_3(H_2O)_2$ in dcm with Φ = 0.21): 55.05±4.7%.

2.20 Synthesis of $Eu(TTA)_3$PIP-2nitro

PIP-2nitro (0.01231 g, 0.003606 mmol, in 5 mL methanol) and $Eu(TTA)_3(H_2O)_2$ (0.03071 g, 0.03606 mmol, in 5 mL methanol) were first mixed together in a 25-50 mL Erlenmeyer flask. The resulting solution was then allowed to stir at 50^{o}C for 30 minutes. Then a septum or cork was placed onto the Erlenmeyer bottom flask and the solution was allowed to stir at room temperature overnight. The solution was then filtered and was allowed to evaporate at room

temperature leaving a crystalline product. UV/vis (DCM): λmax =344 nm , 296nm ,274nm. Fluorescence (DCM, λex=340) : λem = = 615 nm, 594 nm, 580 nm, 676 nm, 540 nm. Fluorescence quantum yield (λex= 340 nm, reference: $Eu(TTA)_3(H_2O)_2$ in dcm with Φ = 0.21): 28.69±2.8%.

2.21 Synthesis of $Eu(TTA)_3$PIP-4nitro

PIP-4nitro (0.01023 g, 0.02997 mmol, in 5 mL methanol) and $Eu(TTA)_3(H_2O)_2$ (0.02552 g, 0.02997 mmol, in 5 mL methanol) were first mixed together in a 25-50 mL Erlenmeyer flask. The resulting solution was then allowed to stir at 50^{o}C for 30 minutes. Then a septum or cork was placed onto the Erlenmeyer bottom flask and the solution was allowed to stir at room temperature overnight. The solution was then filtered and was allowed to evaporate at room temperature leaving a crystalline product. UV/vis (DCM): λmax = 340 nm , 290 nm, 260 nm. Fluorescence (DCM, λex=340) : λem =615 nm, 594 nm, 580 nm, 676 nm. Fluorescence quantum yield (λex= 340 nm, reference: $Eu(TTA)_3(H_2O)_2$ in dcm with Φ = 0.21): 34.64±6.3%.

CHAPTER 3: RESULTS AND DISCUSSION

3.1 Synthesis

The first step in the synthesis process is to produce 1, 10-phenanthroline-5, 6-dione by reacting commercially available 1, 10-phenanthroline with potassium bromide in solution of concentrated sulfuric acid and fuming nitric acid.

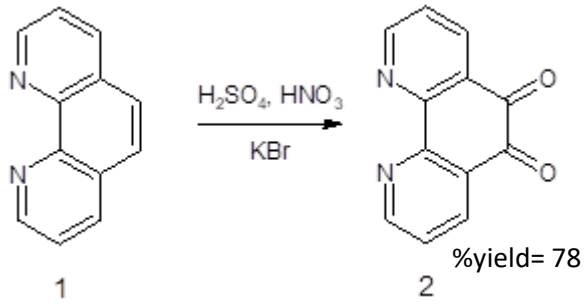

Figure 3. Synthesis of 1, 10-phenanthroline-5, 6-dione

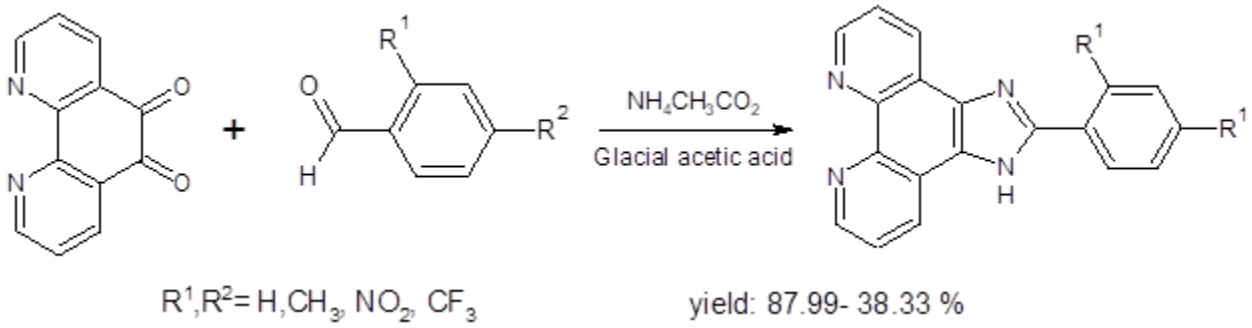

Figure 4**.** Synthesis of 2-phenyl-1H-imidazo[4,5-f][1,10]phenanthroline constituents

For the production of the PIP and its variants, 1, 10-phenanthroline-5, 6-dione (1), made in the previous step, is reacted with a benzaldehyde derivative (3) and ammonium acetate in a glacial acetic acid as shown in

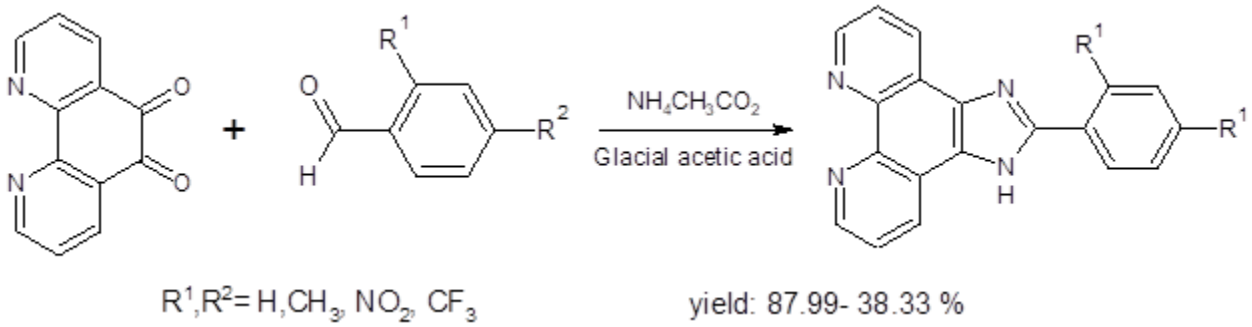

Figure 4. The solution is refluxed and finally neutralized to obtain desired PIP ligand (4). These compounds were then characterized using FT-IR, NMR, and UV-Vis. These steps were all completed for all seven PIP derivatives within this project and these are shown in Figure 5. Surprisingly, out of these seven ligands, the electron-withdrawing gave lower yields with the exception being 2-nitro. With some of the products, such as the 4-nitro and 4-triflouromethyl variants, the acetic acid seemed to remain present creating a tar like substance, this was easily removed with the addition of extra water and more stirring. Those that ended up as tar like substances before the addition of water often gave a lower yield.

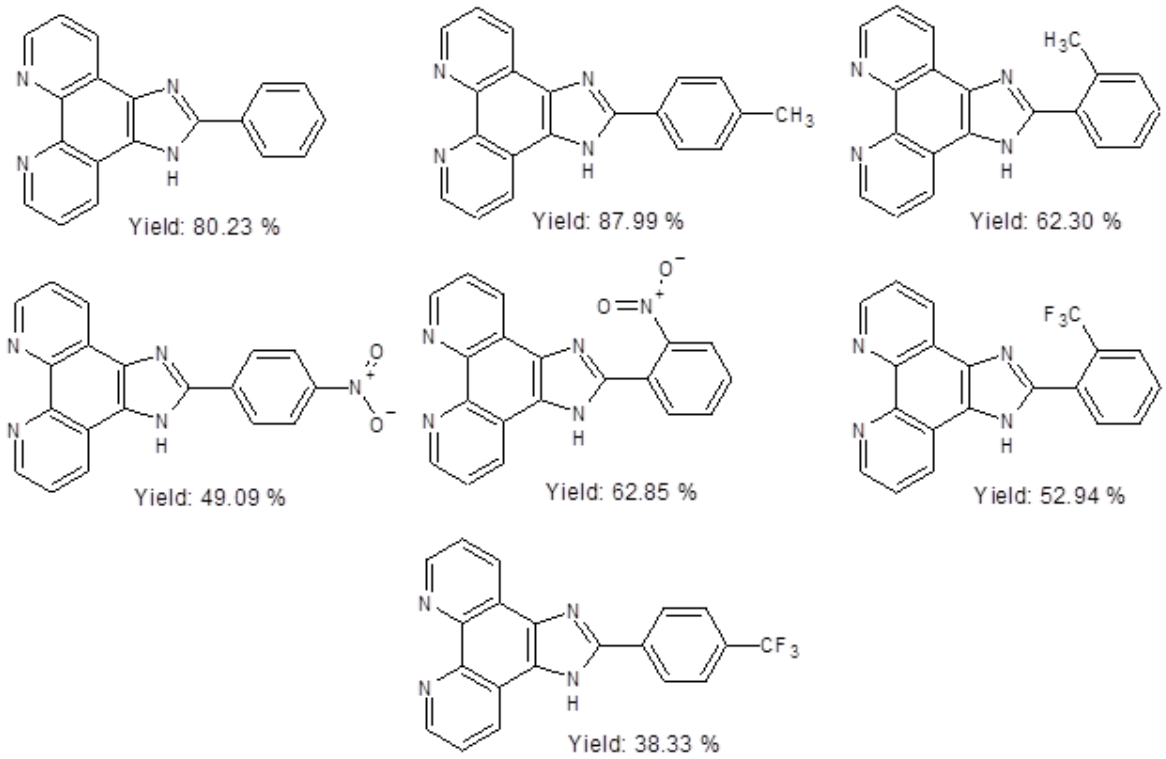

Figure 5. List of PIP Derivatives

To start the synthesis of the planned PIP europium complexes, $Eu(TTA)_3(H_2O)_2$ must be produced. This first europium complex is formed through reacting europium (III) chloride with thenoyltrifluoroacetone (TTA) which will replace the chlorine ions to yield $Eu(TTA)_3(H_2O)_2$ as shown in Figure 6.

Interestingly, the nature of the R group does not seem to have any systematic influence on the yield of the reaction. This was seen in the literature as well.[21] The results that was originally expected was that the electron-withdrawing groups would make the aldehyde starting material more reactive though this was not the case as all reduced yield was attributed to improper neutralization of the acetic acid.

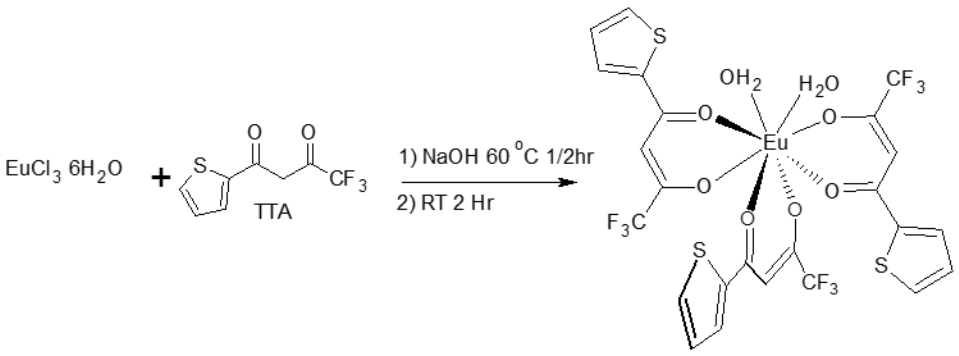

Figure 6. Synthesis of $Eu(TTA)_3(H_2O)_2$

After both the $Eu(TTA)_3(H_2O)_2$ and the PIP ligand are produced both are then dissolved in methanol and stirred at 50°C for 30 minutes then stirred over night to produce the final product as shown in Figure 7. After the product is allowed to crystallize out of the solution, the quantum yield of the complex is calculated using the fluorometer and the UV-Vis spectrometer with $Eu(TTA)_3(H_2O)_2$ as a standard.

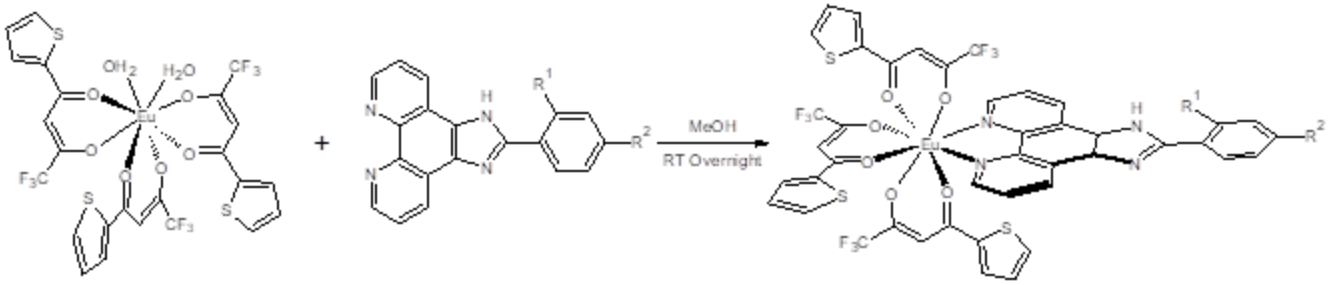

Figure 7. Synthesis of the europium complexes where R^1, R^2= H, CH_3, NO_2, and CF_3

3.2 DFT optimized structures

Shown below in Figure 8 and in Table 1.There are very little differences within all the structures as it is observed that the bonds lengths are nearly identical.

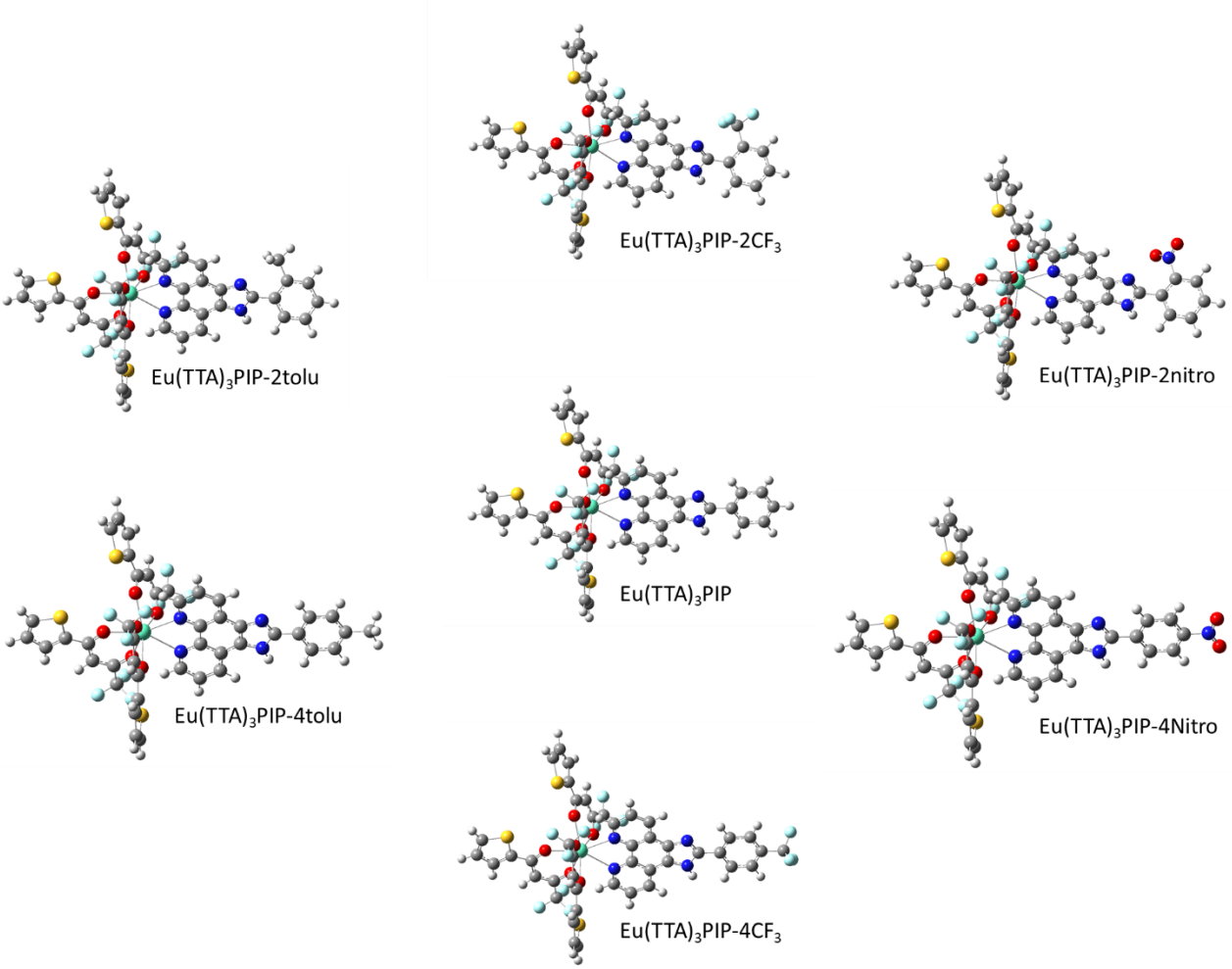

Figure 8. DFT Optimized structures of $Eu(TTA)_3PIP$ complexes

Table 1. Bond distances for the optimized structures

R=	H	2 tolu	4 tolu	2 nitro	4 nitro	2 CF3	4 CF3
EU-N1	2.68119	2.68160	2.68044	2.6833	2.68763	2.68186	2.68465
Eu-N2	2.69703	2.69691	2.69636	2.69801	2.70420	2.69777	2.70083
Eu-O 1	2.39673	2.39672	2.39694	2.39381	2.39554	2.3952	2.3952
Eu-O 2	2.41072	2.41119	2.41087	2.40873	2.40922	2.40993	2.40991
Eu-O 3	2.39802	2.39837	2.39822	2.39854	2.39663	2.3987	2.39711
Eu-O 4	2.42544	2.42491	2.42563	2.42631	2.42399	2.42521	2.42471
Eu-O 5	2.39483	2.39501	2.39556	2.39398	2.39155	2.39449	2.39324
Eu-O 6	2.39358	2.39354	2.39369	2.39544	2.39068	2.39554	2.39196

The only major differences to note is the change in dihedral angles at the imidazole and phenyl groups. While all complexes containing a para functional group on the phenyl ring remain at a 0^o, the complexes containing ortho functional groups on the phenyl ring have varying changes in the dihedral angle based of the size of the attached group. The change in dihedral angle in each of the complexes containing the ortho functional groups can be seen below in Table 2.

Table 2. Dihedral angles of ortho $Eu(TTA)_3PIP$ complexes

Complex	Angle (degrees)
$Eu(TTA)_3PIP$-2tolu	29.83504
$Eu(TTA)_3PIP$-2CF_3	43.69358
$Eu(TTA)_3PIP$-2nitro	45.85544

3.3 Phenyl-1H-imidazo[4,5-f][1,10]phenanthroline and Eu^{3+} Complex

3.3.1 Ultraviolet-Visible Absorption Spectroscopy

The synthesis was considered a success if the UV-Vis spectrum contained peaks for both the PIP and TTA ligands. The TTA has an absorption peak at approximately 340 nm while the PIP ligands had two peaks that ranged from 255-276nm and 281-289nm. The peaks from the PIP ligand also undergo a red shift upon complexing with Eu^{3+} ion which is also indicative of a successful reaction.

The qualitative UV-Vis spectra for PIP along with its respective Eu^{3+} complex is presented in

Figure **9** below. Upon looking at the spectra for the ligand, a strong peak seen at 274 nm becomes quite noticeable. This 274 nm absorption band belongs to the phenanthroline group of the ligand, along with a secondary peak at around 288 nm. Upon being chelation to $Eu(TTA)_3$,

we can also see that the phenanthroline peak is shifted from 274 nm to 280 nm while the peak at 288 nm has become more defined and had shifted to 299 nm. The Eu complex shows a peak at approximately 340 nm belonging to TTA. These shifts from the ligand and the introduction of a 340 nm peak suggest proper chelation to the Eu^{3+} metal ion.

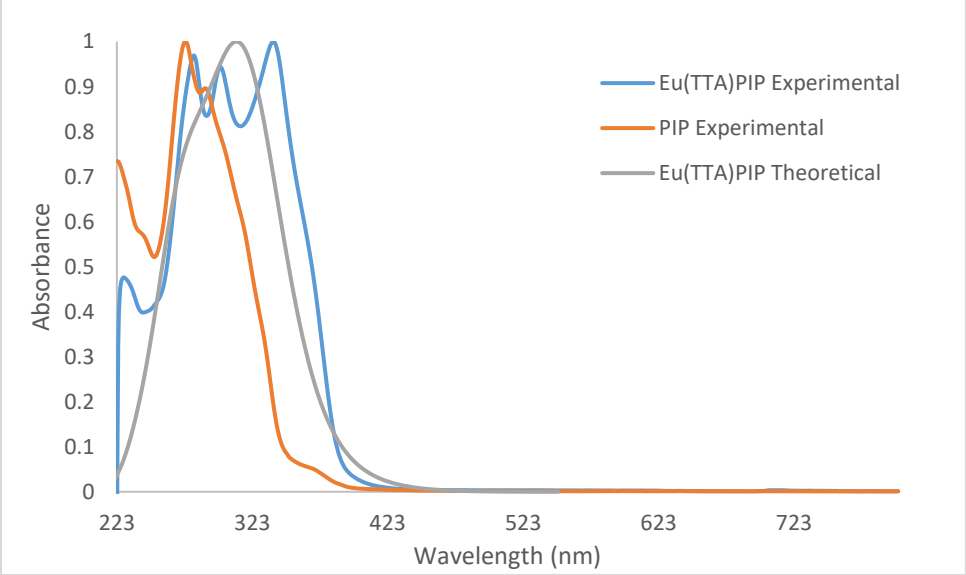

Figure 9. Qualitative Absorption spectra for PIP, its respected Eu complex, and the theoretical spectrum of the complex

When comparing the theoretical and the experimental spectra of the complex it can be seen that the theoretical spectra lacks 2 of the λ_{max} seen in the experimental spectra. For a list of λ_{max} of both theoretical and experimental absorbance data can be seen in Table 3. By looking over the theoretical TDDFT computations the orbitals involved in the theoretical absorption spectra above can be viewed. When evaluating the singlet TDDFT produced by the Gaussian 09

software the molecular orbitals involved the theoretical absorbance spectrum can be observed. The orbitals which are related to the largest λ_{max} max is shown in Figure 10.

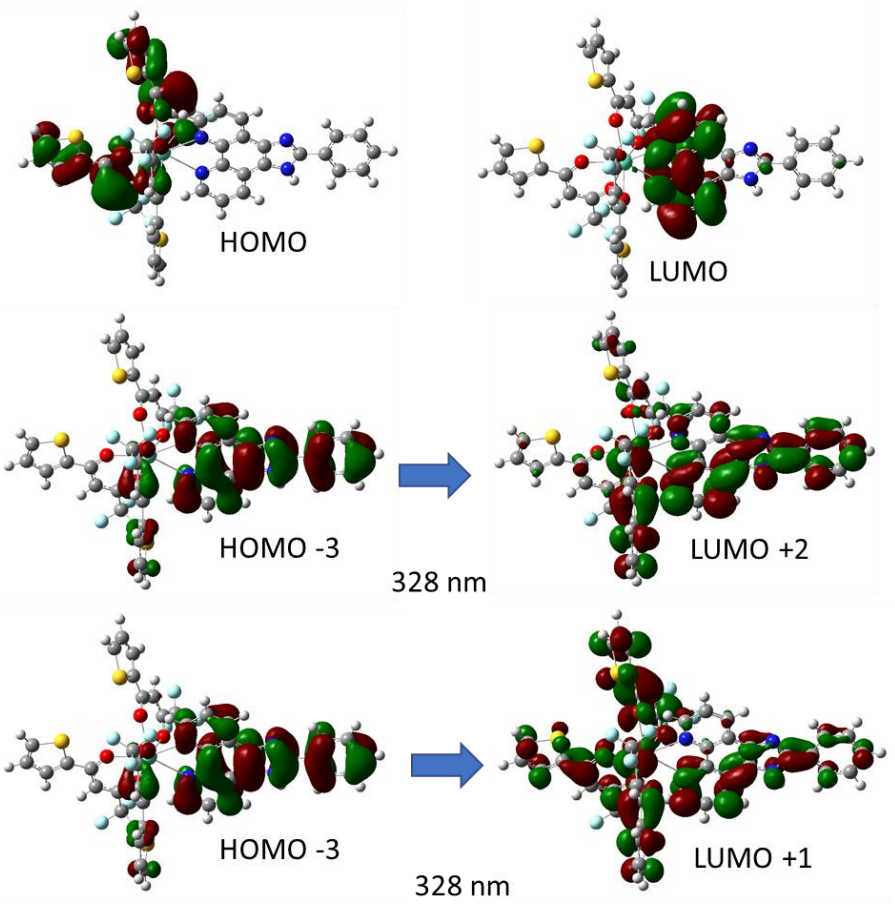

Figure 10. HOMO, LUMO, and the molecular orbitals involved in the theoretical absorptions for $Eu(TTA)_3PIP$

Table 3. λ_{max} values for complexes, both experimental and theoretical.

	Experimental λ_{max} (nm	Theoretical λ_{max} (nm)
$Eu(TTA)_3PIP$	338	328, 315
	299	301
	280	278, 272
	228	241
$Eu(TTA)_3PIP$-2tolu	339	326, 317
	300	296
	281	278, 272 ,266
	226	240
$Eu(TTA)_3PIP$-4tolu	339	332, 321
	297	315, 301
	275	280, 273
	227	245
$Eu(TTA)_3PIP$-2nitro	341	318
	293	294
	271	274, 269
$Eu(TTA)_3PIP$-4nitro	343	317
	294	273
	262	265
	230	257
$Eu(TTA)_3PIP$-2CF_3	340	326, 323
	294	315, 301
	274	269, 268
	244	239
$Eu(TTA)_3PIP$-4CF_3	340	330
	301	316, 310
	298	272
	228	243

3.3.2 Fluorescence Spectra of $Eu(TTA)_3PIP$

The fluorescence spectra for $Eu(TTA)_3PIP$, shown below in Figure 11, shows a strong emission of 615 nm. This emission is a result of the $^5D_0 \rightarrow {}^7F_2$ transition which is strong due to its induced electric dipole transition because of its highly polarizable environment around the Eu^{3+} ion. When comparing it to $Eu(TTA)_3(H_2O)_2$, it can be observed that it retains much of the same

emissions, only really differing in the intensity of the emissions. As can be seen in Figure 11, the intensity of the $Eu(TTA)_3PIP$ at 615 nm shows an increase of 504.69 when compared to $Eu(TTA)_3H_2O$ of similar concentration. The chelated product also showed increased emission intensities at 592 nm and 580, being produced by the $^5D_0 \rightarrow {}^7F_1$ and the $^5D_0 \rightarrow {}^7F_0$ respectively.[22]

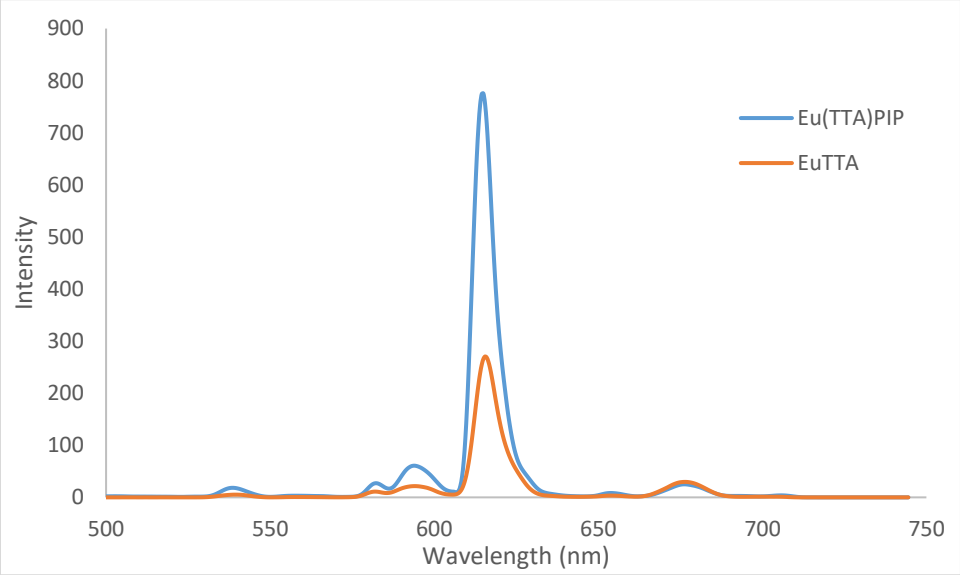

Figure 11. Fluorescence spectra of $Eu(TTA)_3PIP$ and $Eu(TTA)_3(H_2O)_2$

3.4 2-Tolu-1H-imidazo[4,5-f][1,10]phenanthroline and Eu^{3+} Complex

3.4.1 Ultraviolet-Visible Absorption Spectroscopy

The qualitative UV-Vis spectra for PIP-2-tolu along with its respective Eu^{3+} complex is presented in Figure 12 below. Upon looking at the spectra for the ligand, a strong peak seen at 257 nm becomes quite noticeable. This 257 nm absorption band belongs to the phenanthroline group of the ligand, along with a secondary peak at around 288 nm. Upon being chelation to $Eu(TTA)_3$, we can also see that the phenanthroline peak is shifted from 257 nm to 281 nm while the peak at 288 nm has become more defined and had shifted to 300 nm. The peak which was once situated at 240 nm has seemed to merge with what was once the 257 nm absorption upon

being chelated to europium as it is absent within the spectra of the complex. The Eu complex shows a peak at approximately 340 nm belonging to TTA. These shifts from the ligand and the introduction of a 340 nm peak suggest proper chelation to the Eu^{3+} metal ion.

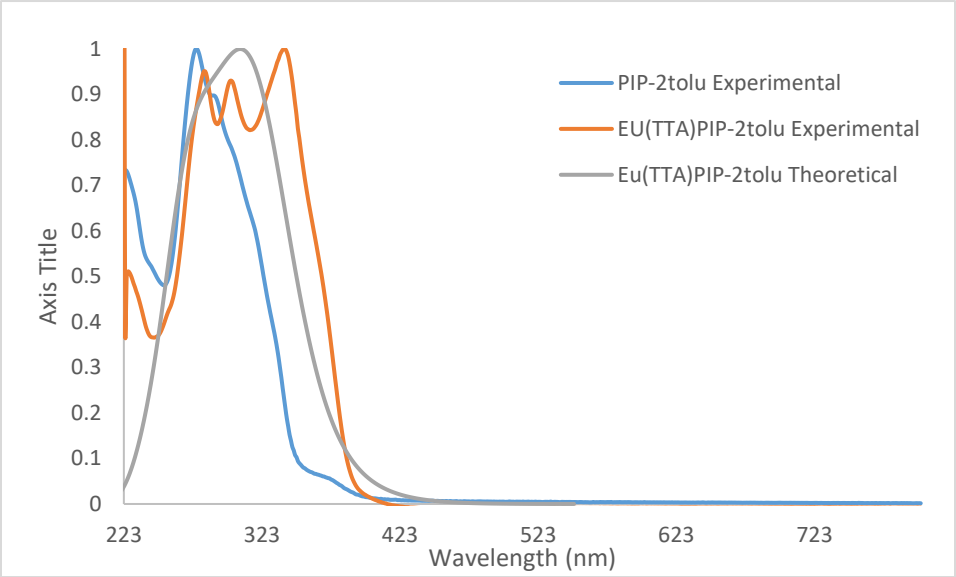

Figure 12. Qualitative absorption for PIP-2tolu, its respected Eu complex, and the theoretical spectrum of the complex

When comparing the theoretical and the experimental spectra of the complex it can be seen that the theoretical spectra lacks 2 of the λ_{max} seen in the experimental spectra. For a list of λ_{max} of both theoretical and experimental absorbance data can be seen in Table 3. By looking over the theoretical TDDFT computations the orbitals involved in the theoretical absorption spectra above can be viewed. When evaluating the singlet TDDFT produced by the Gaussian 09 software the molecular orbitals involved the theoretical absorbance spectrum can be observed. The orbitals which are related to the largest λ_{max} max is shown in Figure 13.

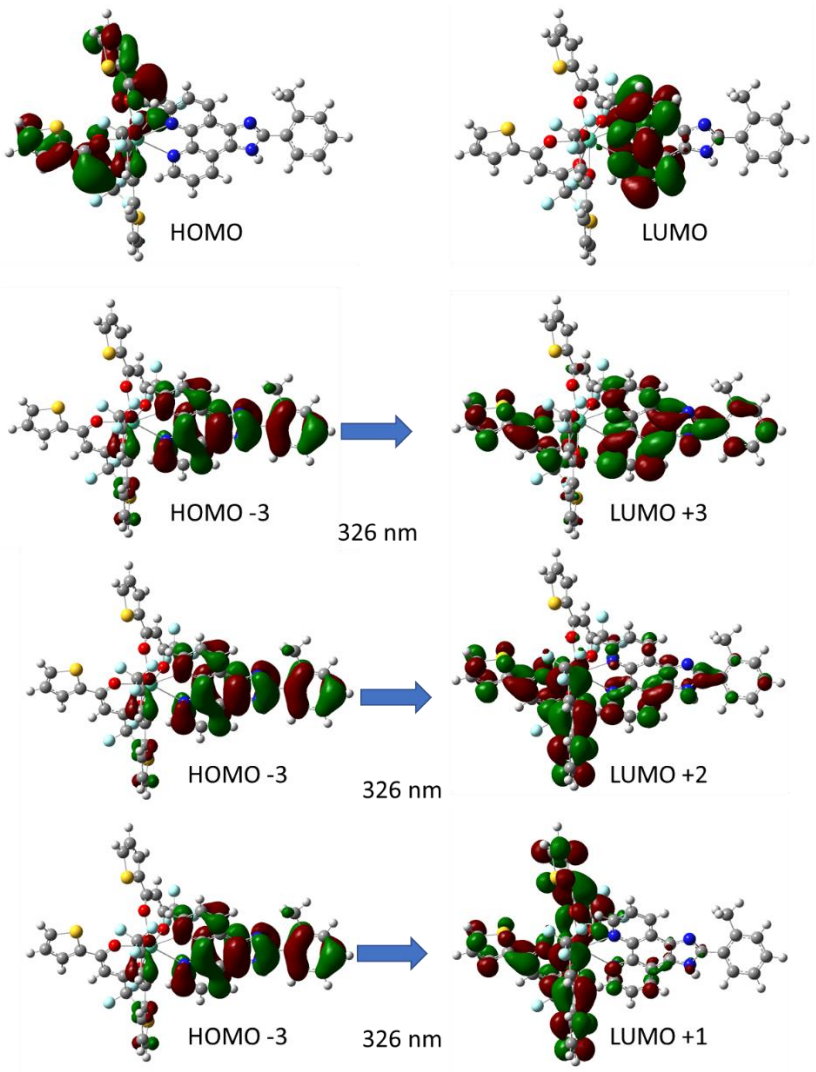

Figure 13. HOMO, LUMO, and the molecular orbitals involved in the theoretical absorptions for $Eu(TTA)_3PIP\text{-}2tolu$

3.4.2 Fluorescence Spectroscopy of $Eu(TTA)_3PIP\text{-}2tolu$

The fluorescence spectra for $Eu(TTA)_3PIP\text{-}2tolu$, shown below in Figure 14, shows a strong emission of 615 nm. This emission is a result of the $^5D_0 \rightarrow {}^7F_2$ transition which is strong due to its induced electric dipole transition because of its highly polarizable environment around the Eu^{3+}

ion. When comparing it to $Eu(TTA)_3(H_2O)_2$, it can be observed that it retains much of the same emissions, only really differing in the intensity of the emissions. As can be seen in Figure 14, the intensity of the $Eu(TTA)_3$PIP-2tolu at 615 nm shows an increase of 481.01 when compared to $Eu(TTA)_3H_2O$ of similar concentration. The chelated product also showed increased emission intensities at 592 nm and 580, being produced by the $^5D_0 \rightarrow {}^7F_1$ and the $^5D_0 \rightarrow {}^7F_0$ respectively.

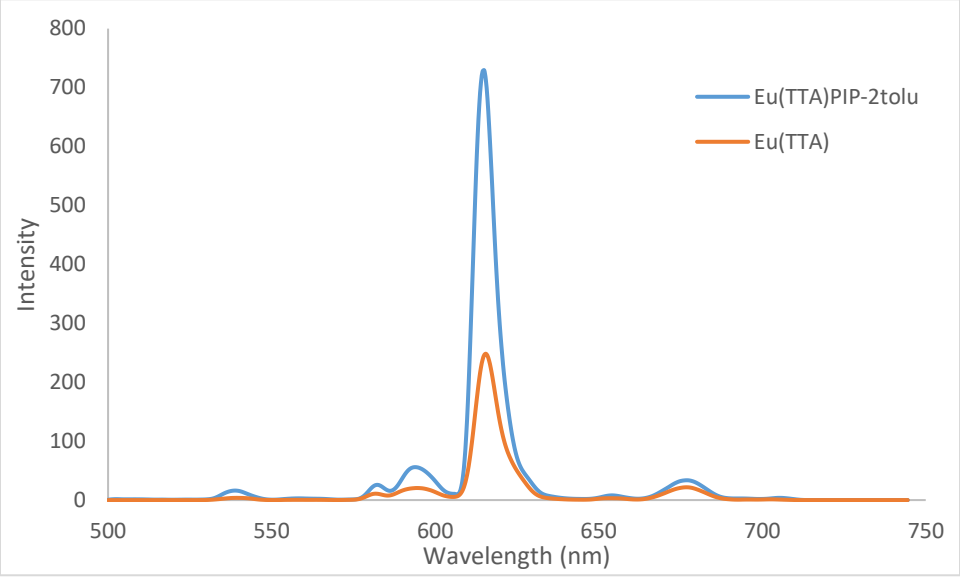

Figure 14. Fluorescence spectra of $Eu(TTA)_3$PIP-2tolu and $Eu(TTA)_3(H_2O)_2$

3.5 4-Tolu-1H-imidazo[4,5-f][1,10]phenanthroline and Eu^{3+} Complex

3.5.1 Ultraviolet-Visible Absorption Spectroscopy

The qualitative UV-Vis spectra for PIP-4tolu along with its respective Eu^{3+} complex is presented in Figure 15 below. Upon looking at the spectra for the ligand, a strong peak seen at 265 nm becomes quite noticeable. This 265 nm absorption band belongs to the phenanthroline group of the ligand, along with a secondary peak at around 283 nm. Upon being chelation to $Eu(TTA)_3$, we can also see that the phenanthroline peak is shifted from 265 nm to 275 nm while the peak at

283 nm has become more defined and had shifted to 297 nm. The Eu complex shows a peak at approximately 340 nm belonging to TTA. These shifts from the ligand and the introduction of a 340 nm peak suggest proper chelation to the Eu^{3+} metal ion.

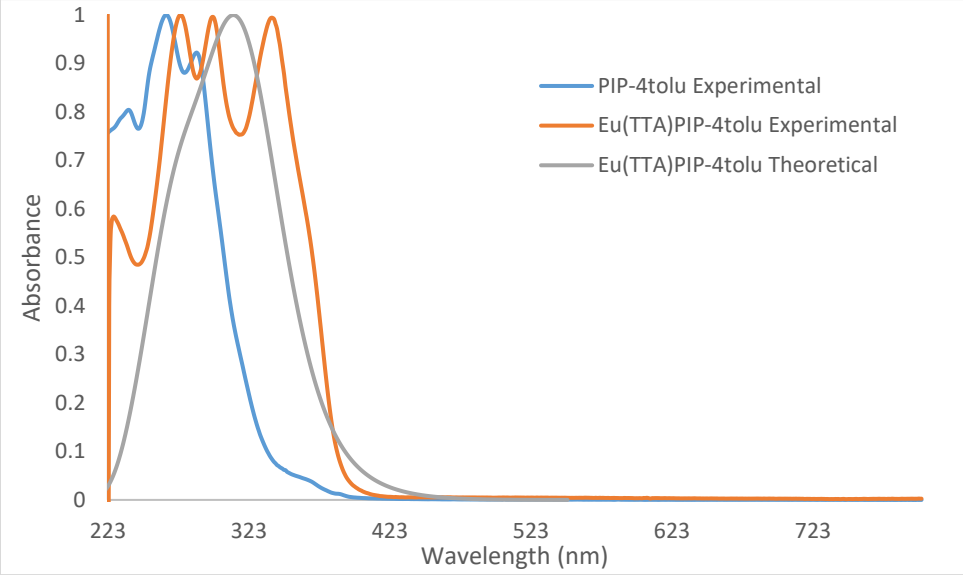

Figure 15. Qualitative absorption for PIP-4tolu, its respected Eu complex, and the theoretical spectrum of the complex

When comparing the theoretical and the experimental spectra of the complex it can be seen that the theoretical spectra lacks 2 of the λ_{max} seen in the experimental spectra. For a list of λ_{max} of both theoretical and experimental absorbance data can be seen in Table 3. By looking over the theoretical TDDFT computations the orbitals involved in the theoretical absorption spectra above can be viewed. When evaluating the singlet TDDFT produced by the Gaussian 09 software the molecular orbitals involved the theoretical absorbance spectrum can be observed. The orbitals which are related to the largest λ_{max} max is shown in Figure 16.

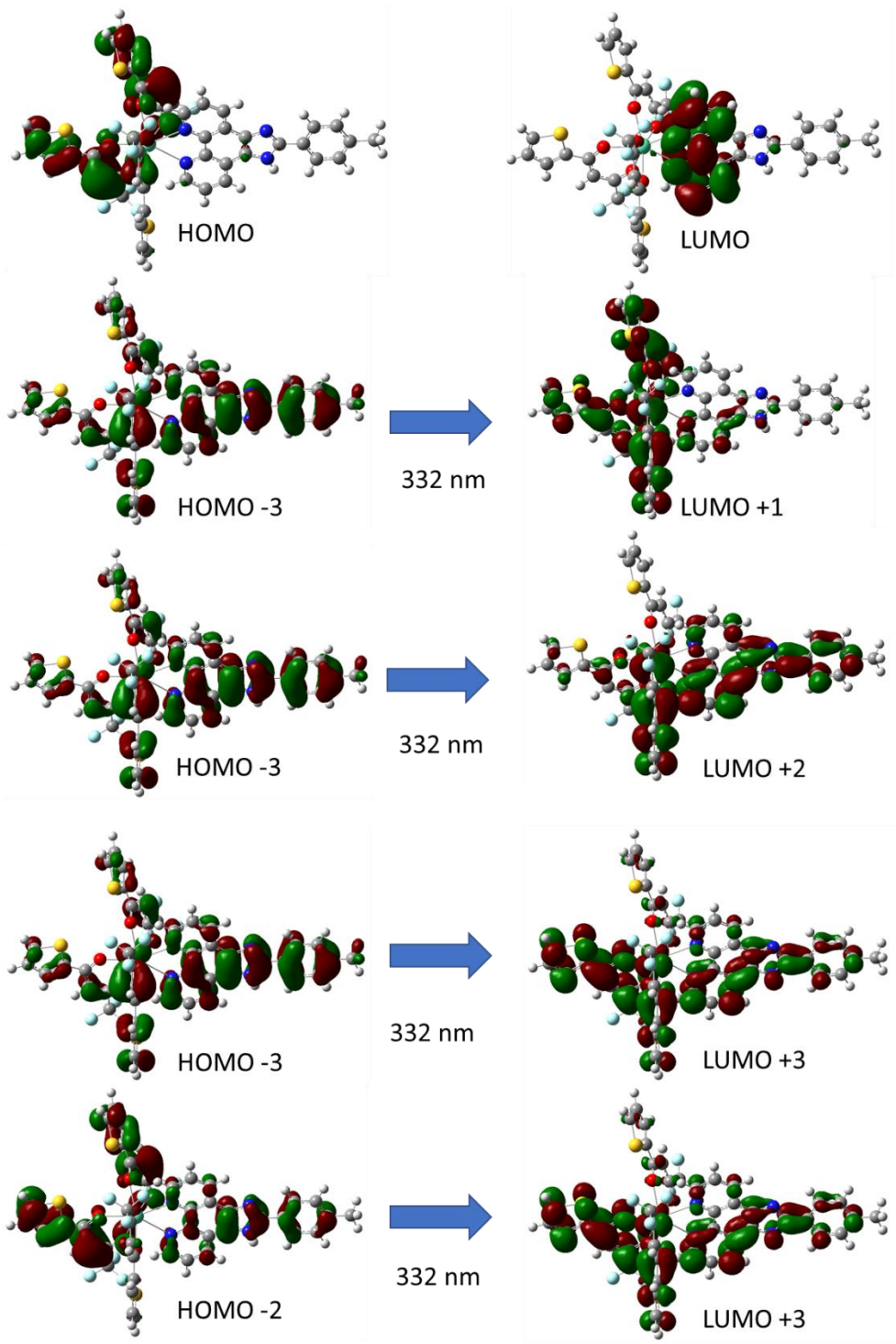

Figure 16. HOMO, LUMO, and the molecular orbitals involved in the theoretical absorptions for $Eu(TTA)_3PIP$-4tolu

3.5.2 Fluorescence Spectra of $Eu(TTA)_3PIP$-4tolu

The fluorescence spectra for $Eu(TTA)_3PIP$-4tolu, shown below in Figure 17,shows a strong emission of 615 nm. This emission is a result of the $^5D_0 \rightarrow {}^7F_2$ transition which is strong due to its induced electric dipole transition because of its highly polarizable environment around the Eu^{3+} ion. When comparing it to $Eu(TTA)_3(H_2O)_2$, it can be observed that it retains much of the same emissions, only really differing in the intensity of the emissions. As can be seen in Figure 17, the intensity of the $Eu(TTA)_3PIP$-4-olu at 615 nm shows an increase of 624.06 when compared to $Eu(TTA)_3H_2O$ of similar concentration. The chelated product also showed increased emission intensities at 592 nm and 580, being produced by the $^5D_0 \rightarrow {}^7F_1$ and the $^5D_0 \rightarrow {}^7F_0$ respectively.

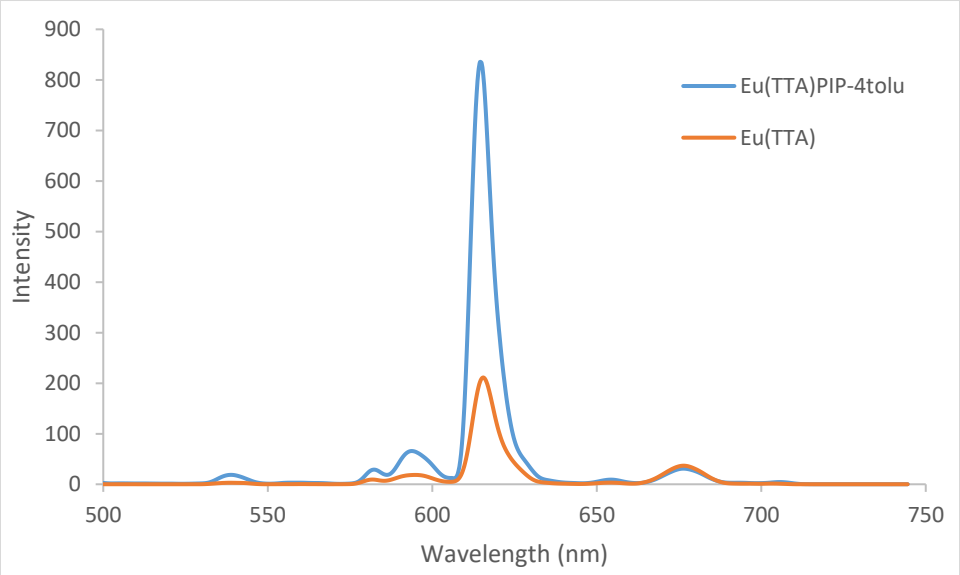

Figure 17. Fluorescence spectra of $Eu(TTA)_3PIP$-4tolu and $Eu(TTA)_3(H_2O)_2$

3.6 [2-triflouromethy-phenyl]-1H-imidazo[4,5-f][1,10]phenanthroline and Eu^{3+} Complex

3.6.1 Ultraviolet-Visible Absorption Spectroscopy

The qualitative UV-Vis spectra for PIP-2CF_3 along with its respective Eu^{3+} complex is presented in Figure 18 below. Upon looking at the spectra for the ligand, a strong peak seen at 242 nm becomes quite noticeable. This 242 nm absorption band belongs to the phenanthroline group of the ligand, this band has seemed to be shifted due to the CF_3 pulling electron density from the phenanthroline. The usual secondary peak has been relatively unaffected, being situated at 284 nm. Upon being chelation to $Eu(TTA)_3$, we can also see that the phenanthroline peak is shifted from 242 nm to 277 nm while the peak at 284 nm has become more defined and had shifted to 294 nm. The Eu complex shows a peak at approximately 340 nm belonging to TTA. These shifts from the ligand and the introduction of a 340 nm peak suggest proper chelation to the Eu^{3+} metal ion.

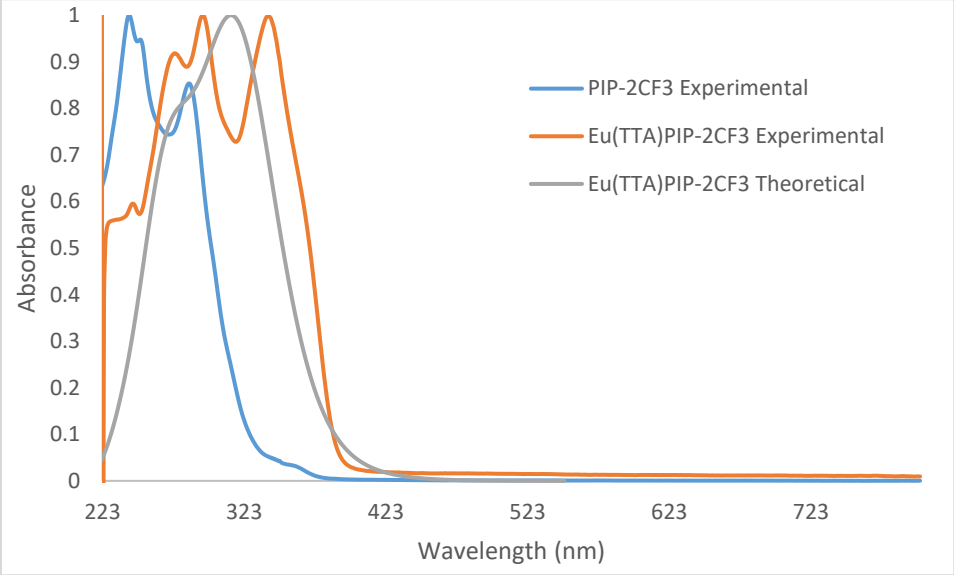

Figure 18. Qualitative absorption for PIP-2CF_3, its respected Eu complex, and the theoretical spectrum of the complex

When comparing the theoretical and the experimental spectra of the complex it can be seen that the theoretical spectra lacks 2 of the λ_{max} seen in the experimental spectra. For a list of

λ_{max} of both theoretical and experimental absorbance data can be seen in Table 3 . By looking over the theoretical TDDFT computations the orbitals involved in the theoretical absorption spectra above can be viewed When evaluating the singlet TDDFT produced by the Gaussian 09 software the molecular orbitals involved the theoretical absorbance spectrum can be observed. The orbitals which are related to the largest λ_{max} max is shown in Figure 20

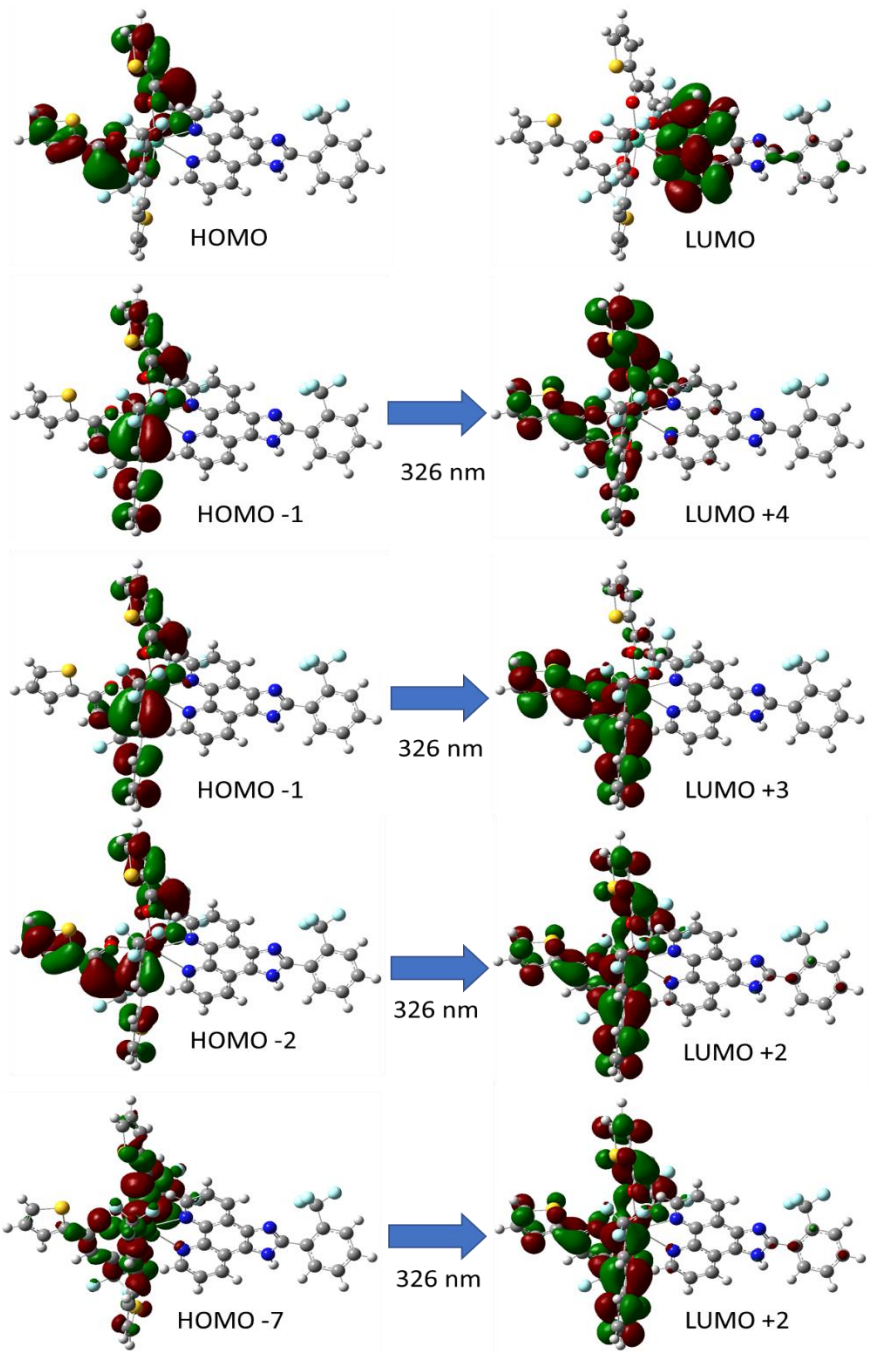

Figure 19. HOMO, LUMO, and the molecular orbitals involved in the theoretical absorptions for $Eu(TTA)_3PIP\text{-}2CF_3$

3.6.2 Fluorescence Spectra of $Eu(TTA)_3PIP\text{-}2CF_3$

The fluorescence spectra for $Eu(TTA)_3PIP\text{-}2CF_3$, shown below in Figure 20, shows a strong emission of 615 nm. This emission is a result of the $^5D_0 \rightarrow {}^7F_2$ transition which is strong due to its induced electric dipole transition because of its highly polarizable environment around the Eu^{3+} ion. When comparing it to $Eu(TTA)_3(H_2O)_2$, it can be observed that it retains much of the same emissions, only really differing in the intensity of the emissions. As can be seen in Figure 20, the intensity of the $Eu(TTA)_3PIP\text{-}2CF_3$ at 615 nm shows an increase of 538.94 when compared to $Eu(TTA)_3H_2O$ of similar concentration. The chelated product also showed increased emission intensities at 592 nm and 580, being produced by the $^5D_0 \rightarrow {}^7F_1$ and the $^5D_0 \rightarrow {}^7F_0$ respectively.

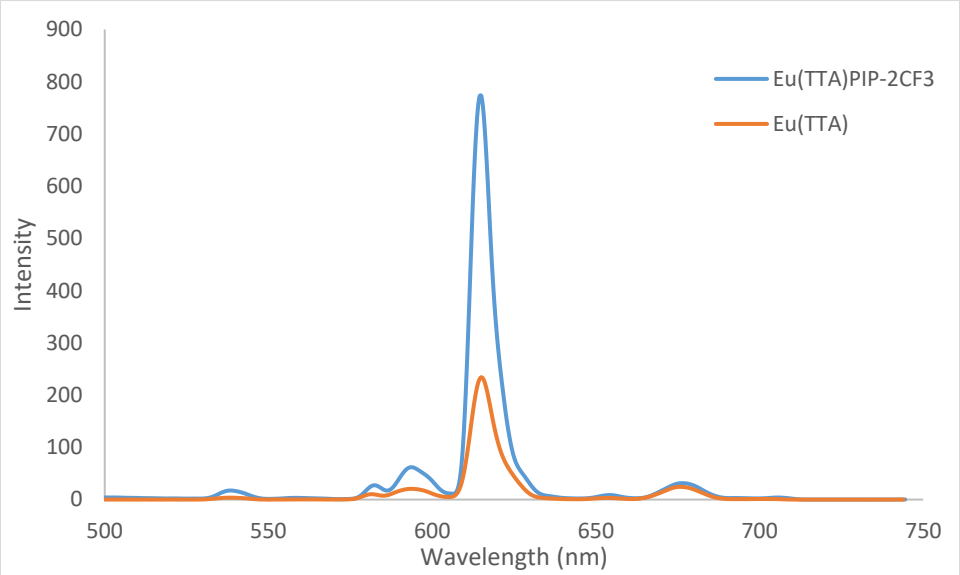

Figure 20. Fluorescence spectra of $Eu(TTA)_3PIP\text{-}2CF_3$ and $Eu(TTA)_3(H_2O)_2$

3.7 [4-triflouromethy-phenyl]-1H-imidazo[4,5-f][1,10]phenanthroline and Eu^{3+} Complex

3.7.1 Ultraviolet-Visible Absorption Spectroscopy

The qualitative UV-Vis spectra for $PIP\text{-}4CF_3$ along with its respective Eu^{3+} complex is presented in Figure 21 below. Upon looking at the spectra for the ligand, a strong peak seen at 276 nm becomes quite noticeable. This 276 nm absorption band belongs to the phenanthroline group of

the ligand, along with a secondary peak at around 289 nm and a third peak can be seen at 319 nm. Upon being chelation to $Eu(TTA)_3$, we can also see that the phenanthroline peak is shifted from 276 nm to 282 nm while the peak at 289 nm has become more defined and had shifted to 298 nm. The Eu complex shows a peak at approximately 340 nm belonging to TTA, the 319 nm peak seen in the ligand spectra can be seen somewhat merged with it. These shifts from the ligand and the introduction of a 340 nm peak suggest proper chelation to the Eu^{3+} metal ion.

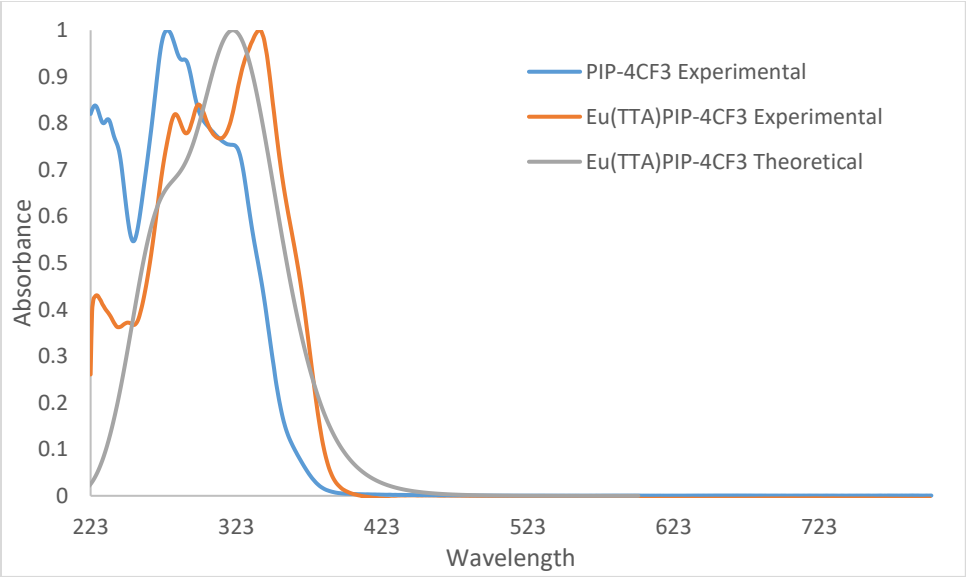

Figure 21. Qualitative absorption for PIP-$4CF_3$, its respected Eu complex, and the theoretical spectrum of the complex

When comparing the theoretical and the experimental spectra of the complex it can be seen that the theoretical spectra lacks 2 of the λ_{max} seen in the experimental spectra. For a list of λ_{max} of both theoretical and experimental absorbance data can be seen in Table 3. By looking over the theoretical TDDFT computations the orbitals involved in the theoretical absorption spectra above can be viewed. When evaluating the singlet TDDFT produced by the Gaussian 09

software the molecular orbitals involved the theoretical absorbance spectrum can be observed. The orbitals which are related to the largest λ_{max} max is shown in Figure 22.

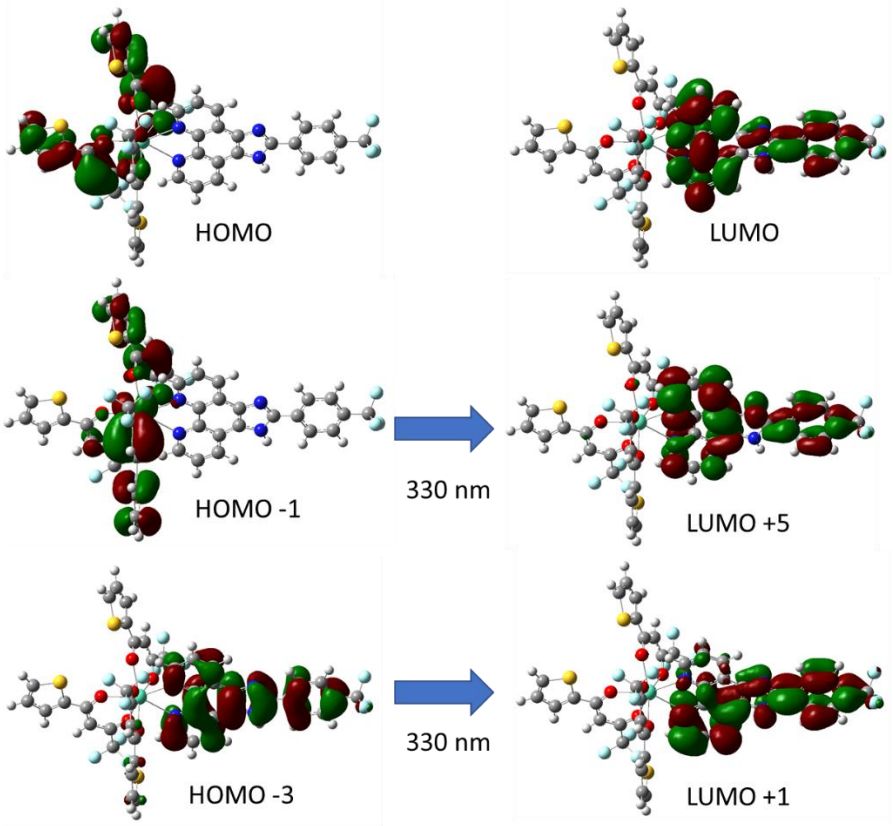

Figure 22. HOMO, LUMO, and the molecular orbitals involved in the theoretical absorptions for $Eu(TTA)_3PIP\text{-}4CF_3$

3.7.2 Fluorescence Spectra of $Eu(TTA)_3PIP\text{-}4CF_3$

The fluorescence spectra for $Eu(TTA)_3PIP\text{-}4CF_3$, shown below in Figure 23, shows a strong emission of 615 nm. This emission is a result of the $^5D_0 \rightarrow {}^7F_2$ transition which is strong due to its induced electric dipole transition because of its highly polarizable environment around the Eu^{3+} ion. When comparing it to $Eu(TTA)_3(H_2O)_2$, it can be observed that it retains much of the same

emissions, only really differing in the intensity of the emissions. As can be seen in Figure 23, the intensity of the $Eu(TTA)_3PIP\text{-}4CF_3$ at 615 nm shows an increase of 436.19 when compared to $Eu(TTA)_3H_2O$ of similar concentration. The chelated product also showed increased emission intensities at 592 nm and 580, being produced by the $^5D_0 \rightarrow {}^7F_1$ and the $^5D_0 \rightarrow {}^7F_0$ respectively.

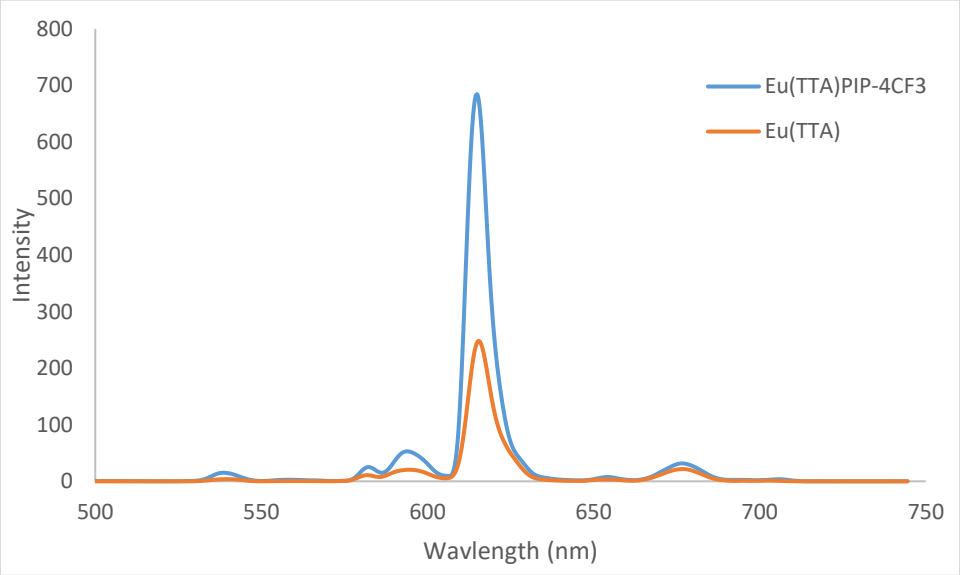

Figure 23. Fluorescence spectra of $Eu(TTA)_3PIP\text{-}4CF_3$ and $Eu(TTA)_3(H_2O)_2$

3.8 [2-nitro-phenyl]-1H-imidazo[4,5-f][1,10]phenanthroline and Eu^{3+} Complex

3.8.1 Ultraviolet-Visible Absorption Spectroscopy

The qualitative UV-Vis spectra for PIP-2nitro along with its respective Eu^{3+} complex is presented in Figure 24 below. Upon looking at the spectra for the ligand, a strong peak seen at 257 nm becomes quite noticeable. This 257 nm absorption band belongs to the phenanthroline group of the ligand, this band has seemed to be shifted due to the NO_2 pulling electron density from the phenanthroline. The usual secondary peak has been relatively unaffected, being situated at 284 nm and a third peak can be seen at 240 nm. Upon being chelation to $Eu(TTA)_3$, we can also see that the phenanthroline peak is shifted from 257 nm to 273 nm while the peak at 284 nm

has become more defined and had shifted to 293 nm. The peak at 240 nm in the ligand spectra is absent in the spectra of the complex, being presumably merged with the peak at 273 nm . The Eu complex shows a peak at approximately 340 nm belonging to TTA. These shifts from the ligand and the introduction of a 340 nm peak suggest proper chelation to the Eu^{3+} metal ion.

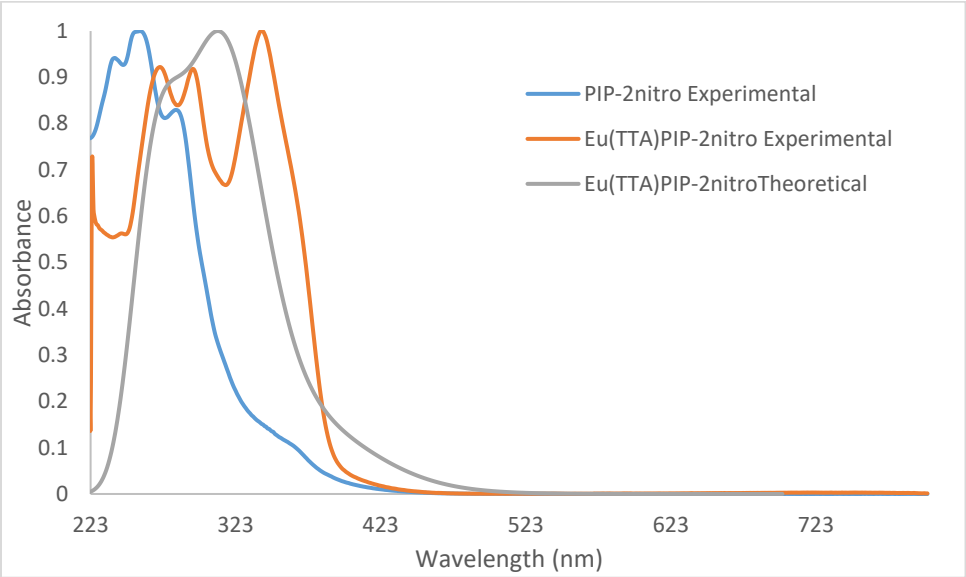

Figure 24. Qualitative absorption for PIP-2nitro, its respected Eu complex, and the theoretical spectrum of the complex

When comparing the theoretical and the experimental spectra of the complex it can be seen that the theoretical spectra lacks 2 of the λ_{max} seen in the experimental spectra. For a list of λ_{max} of both theoretical and experimental absorbance data can be seen in Table 3. By looking over the theoretical TDDFT computations the orbitals involved in the theoretical absorption spectra above can be viewed. When evaluating the singlet TDDFT produced by the Gaussian 09 software the molecular orbitals involved the theoretical absorbance spectrum can be observed. The orbitals which are related to the largest λ_{max} max is shown in Figure 25.

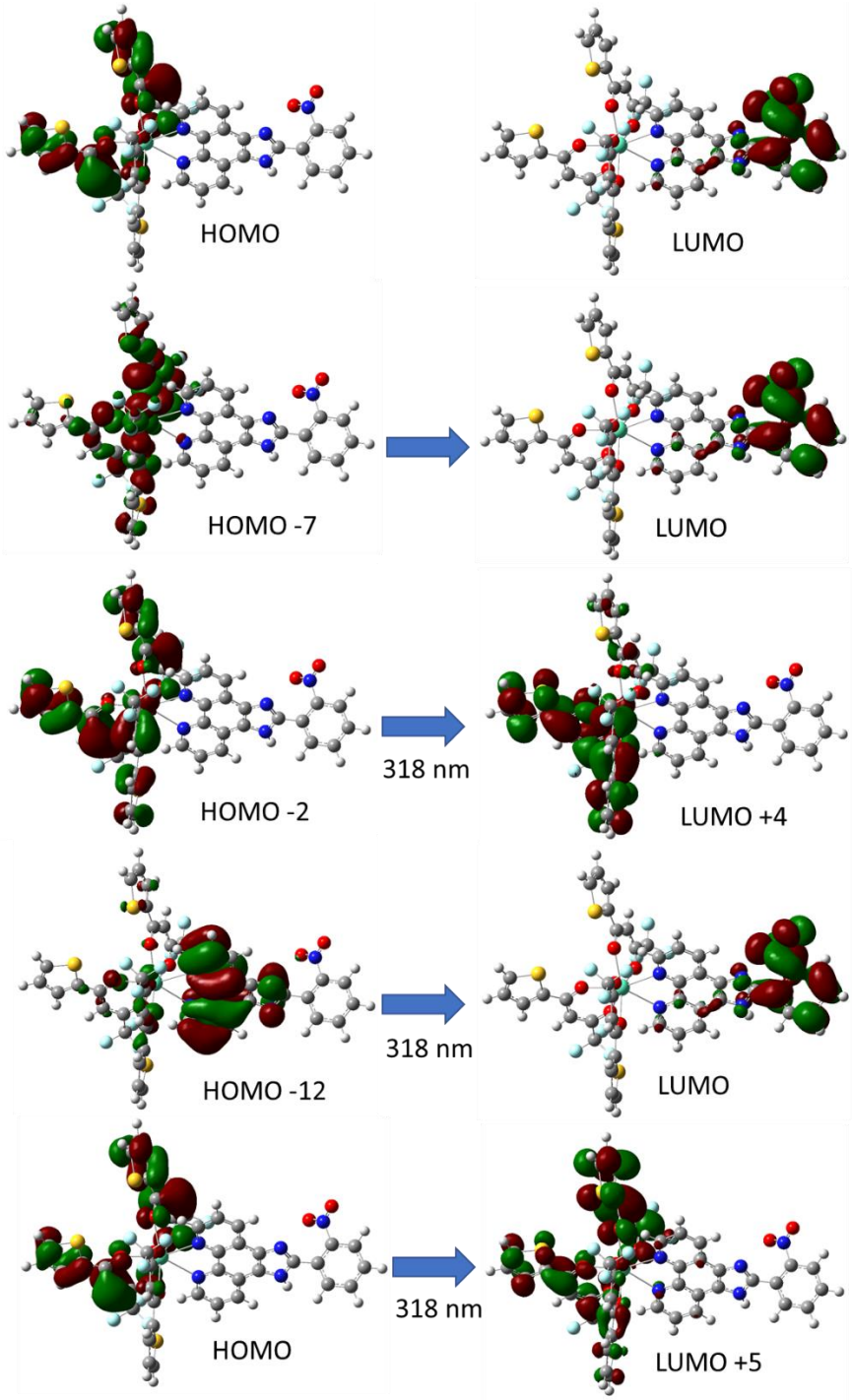

Figure 25. HOMO, LUMO, and the molecular orbitals involved in the theoretical absorptions for $Eu(TTA)_3PIP\text{-}2nitro$

3.8.2 Fluorescence Spectra of $Eu(TTA)_3PIP\text{-}2nitro$

The fluorescence spectra for $Eu(TTA)_3PIP$-2nitro, shown below in Figure 26, shows a strong emission of 615 nm. This emission is a result of the $^5D_0 \rightarrow {}^7F_2$ transition which is strong due to its induced electric dipole transition because of its highly polarizable environment around the Eu^{3+} ion. When comparing it to $Eu(TTA)_3(H_2O)_2$, it can be observed that it retains much of the same emissions, only really differing in the intensity of the emissions. As can be seen in Figure 26, the intensity of the $Eu(TTA)_3PIP$-2nitro at 615 nm shows an increase of 115.15 when compared to $Eu(TTA)_3H_2O$ of similar concentration. The chelated product also showed increased emission intensities at 592 nm and 580, being produced by the $^5D_0 \rightarrow {}^7F_1$ and the $^5D_0 \rightarrow {}^7F_0$ respectively.

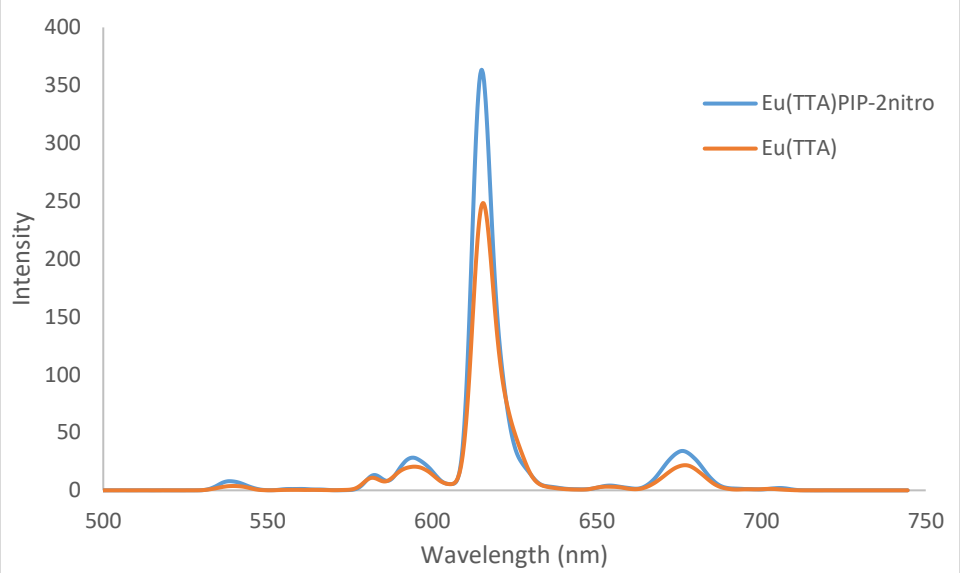

Figure 26. Fluorescence spectra of $Eu(TTA)_3PIP$-2nitro and $Eu(TTA)_3(H_2O)_2$

3.9 [4-nitro-phenyl]-1H-imidazo[4,5-f][1,10]phenanthroline and Eu^{3+} Complex

3.9.1 Ultraviolet-Visible Absorption Spectroscopy

The qualitative UV-Vis spectra for PIP-4nitro along with its respective Eu^{3+} complex is presented in Figure 27 below. Upon looking at the spectra for the ligand, a strong peak seen at 255 nm becomes quite noticeable. This 255 nm absorption band belongs to the phenanthroline

group of the ligand, along with a secondary peak at around 281 nm and a third peak could be seen at 234 nm. Another broad peak can be observed at 369 nm which has not been seen on any of the other ligand spectra, this suggests an impurity is present however no major impurity has been found in the NMR spectrum. Upon being chelation to $Eu(TTA)_{3,}$ we can also see that the phenanthroline peak had slight shift from 255 nm to 262 nm while the peak at 281 nm has become more defined and had shifted to 294 nm. The unknown 369 nm peak has also vanished from the chelated product suggestion later steps had removed it in the complexing reaction. The Eu complex shows a peak at approximately 340 nm belonging to TTA. These shifts from the ligand and the introduction of a 340 nm peak suggest proper chelation to the Eu^{3+} metal ion.

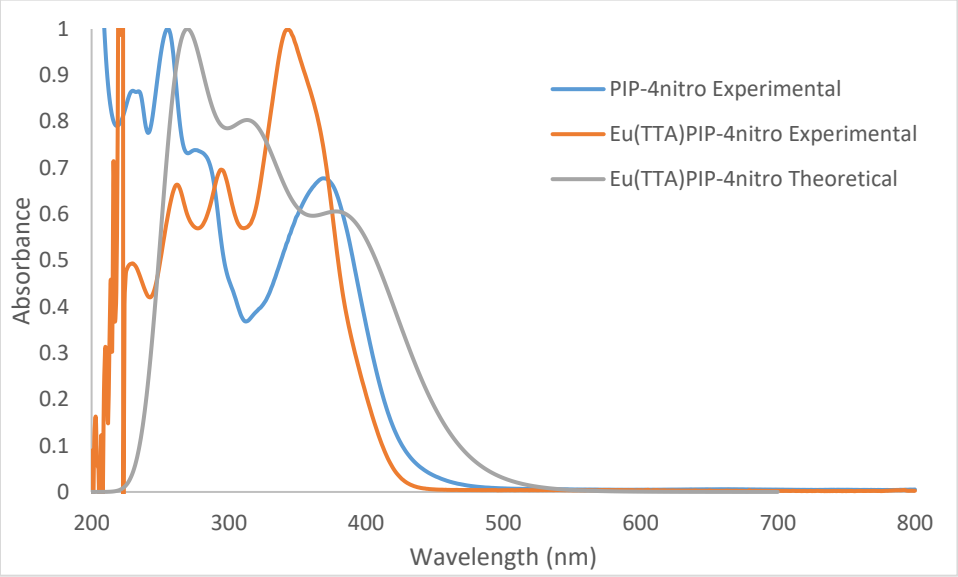

Figure 27. Qualitative absorption for PIP-4nitro, its respected Eu complex, and the theoretical spectrum of the complex

When comparing the theoretical and the experimental spectra of the complex it can be seen that the λ_{max} of the theoretical spectra seems slightly skewed with differing intensities or closer to that of ligand spectra with the inclusion of the 369 peak. For a complete list of λ_{max} of

both theoretical and experimental absorbance data can be seen in Table 3. By looking over the theoretical TDDFT computations the orbitals involved in the theoretical absorption spectra above can be viewed. When evaluating the singlet TDDFT produced by the Gaussian 09 software the molecular orbitals involved the theoretical absorbance spectrum can be observed. The orbitals which are related to the largest λ_{max} max is shown in.

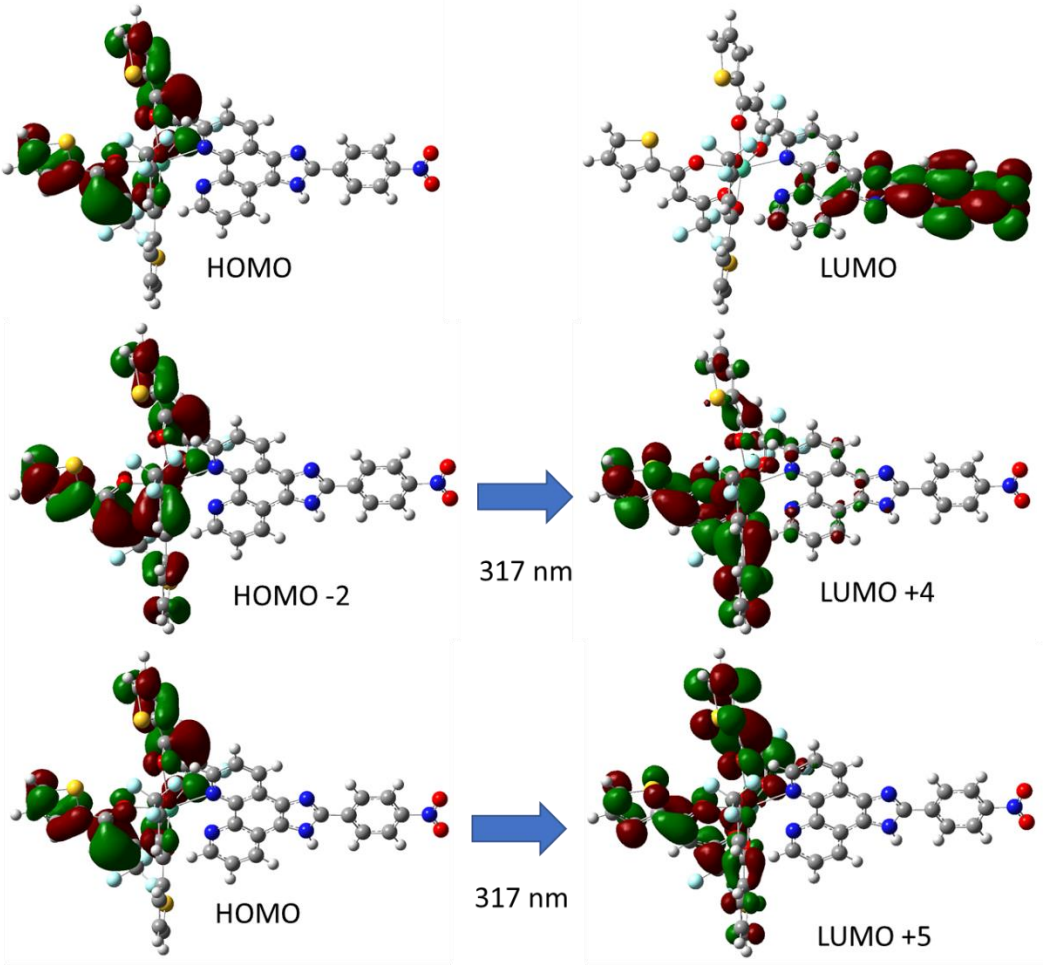

Figure 28. HOMO, LUMO, and the molecular orbitals involved in the theoretical absorptions for EU(TTA)$_3$PIP-4nitro

3.9.2 Fluorescence Spectra of Eu(TTA)$_3$PIP-4nitro

The fluorescence spectra for $Eu(TTA)_3PIP$-4nitro, shown below in Figure 29, shows a strong emission of 615 nm. This emission is a result of the $^5D_0 \rightarrow {}^7F_2$ transition which is strong due to its induced electric dipole transition because of its highly polarizable environment around the Eu^{3+} ion. When comparing it to $Eu(TTA)_3(H_2O)_2$, it can be observed that it retains much of the same emissions, only really differing in the intensity of the emissions. As can be seen in Figure 29, the intensity of the $Eu(TTA)_3PIP$-4nitro at 615 nm shows an increase of 398.73 when compared to $Eu(TTA)_3H_2O$ of similar concentration. The chelated product also showed increased emission intensities at 592 nm and 580, being produced by the $^5D_0 \rightarrow {}^7F_1$ and the $^5D_0 \rightarrow {}^7F_0$ respectively. A tail extending from 500-575 nm which has not been observed in any of the previous complexes is quite evident in the fluorescence spectra, in future project with this sample it may be best to extend the range of detection to 400 or 450 nm in order to get a better look at what is going on.

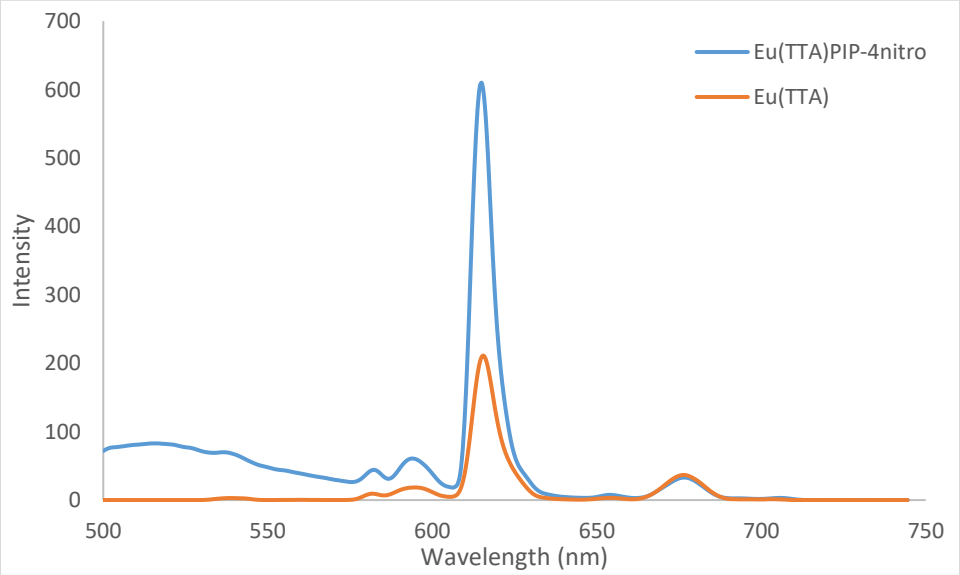

Figure 29. Fluorescence spectra of $Eu(TTA)_3PIP$-4nitro and $Eu(TTA)_3(H_2O)_2$

3.10 Quantum yield values

Table 4. Luminescent Quantum Yield Values of $Eu(TTA)_3PIP$ Complexes

Complex	Φ%	Stdev
$Eu(TTA)_3PIP$	46.14	3.0
$Eu(TTA)_3PIP$-2tolu	61.78	7.5
$Eu(TTA)_3PIP$-4tolu	60.80	7.4
$Eu(TTA)_3PIP$-2nitro	28.69	2.8
$Eu(TTA)_3PIP$-4nitro	34.64	6.3
$Eu(TTA)_3PIP$-$2CF_3$	60.03	8.5
$Eu(TTA)_3PIP$-$4CF_3$	55.06	4.7

Before the initial experiments, it was predicted that by adding electron-donating or withdrawing groups that the quantum yield values would go up and down respectively, but this was found not to be partially correct. As seen in Table 4, when PIP had no added functional groups an initial quantum yield of 46.14% though when adding a functional group the phenyl, not including NO_2, there was an increase in the quantum yield of the final complexes. As only NO_2 seems to forego this trend, it can be suggested that having a powerful electron-withdrawing group affecting the π system will decrease the quantum efficiency. By looking back and Table 2 and comparing it with Table 4, we can see that the dihedral angel of the phenyl function groups does not have any affect on the luminescent quantum yield.

Since there is a known correlation in the luminescent quantum yields of lanthanides and their singlet and triplet state energies, the data from the TDDFT calculations were assessed. From the data, the inter system crossing energy (ΔE_{ISC}) and the energy transfer to the Eu f-orbital (ΔE_{ET}) were calculated and are shown in Table 5. When going over Table 5 there doesn't appear to be any correlation between ΔE_{ET} and the luminescent quantum yield as complexes have similar ΔE_{ET} values with the exception of $Eu(TTA)_3PIP$-4nitro which was significantly lower than the rest. However, the data ISC has a significant variation depending on the substituent

group. Therefore , the variation in the luminescent quantum yield may be a result of the variation of the singlet energy levels. The observed trend between the ΔE_{ISC} and quantum yield (Φ) can be more easily observed in Figure 30. It is observed that between an ΔE_{ISC} of 0.73-0.76 eV that there is an increase in the quantum efficiency suggesting that this range may be the optimal ISC energy gap for this series of complexes. The complexes with larger and lower ΔE_{ISC} than this range were shown to have a lower quantum yield. This can be seen in the data as both $Eu(TTA)_3PIP$ which has a ΔE_{ISC} of 0.8099 and $Eu(TTA)_3PIP\text{-}4CF_3$ with a ΔE_{ISC} of 0.6919 gave the lower quantum yield percentage 46.14 and 55.06% respectively.

Table 5. TDDFT Relative Energy Differences (eV)

Complex	ΔE_{ISC} (eV)	ΔE_{ET} (eV)	Φ%
$Eu(TTA)_3PIP$	0.8099	0.32717	46.14±3.0
$Eu(TTA)_3PIP\text{-}2tolu$	0.7527	0.32777	61.78±7.5
$Eu(TTA)_3PIP\text{-}4tolu$	0.7551	0.32757	60.80±7.3
$Eu(TTA)_3PIP\text{-}2nitro$	0.4661	0.32527	28.69±2.8
$Eu(TTA)_3PIP\text{-}4nitro$	0.2830	0.28097	34.64±6.3
$Eu(TTA)_3PIP\text{-}2CF_3$	0.7342	0.32627	60.03±8.5
$Eu(TTA)_3PIP\text{-}4CF_3$	0.6919	0.32757	55.06±4.7

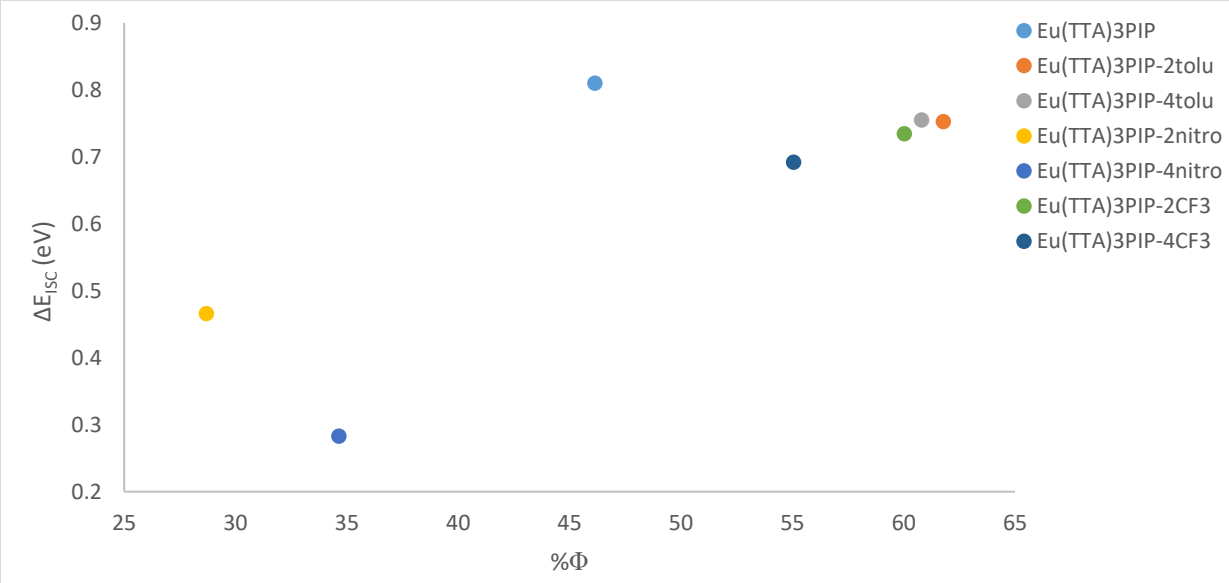

Figure 30. Correlation of the Intersystem Crossing Energy and Luminescent Quantum Yield for the $Eu(TTA)_3PIP$ complexes.

3.11 Future Work

For the future work of this project there are two possible routes in mind, the first being to look over more possible functional groups in order to better confirm the finding in these experiments. For the first route there were a few functional groups that were originally planned to be tested though dropped due to time constraints, one of those being NH_2 which would have been a stronger electron-donating group in the tested series. In order to know for certain that the π system of the phenyl group has an affect on the quantum yield of the complex, the inclusion of meta functional groups and their affects should be included. Another change that would be suggested would be to use a higher level of theory in the theoretical calculations such as the 6-311G (d,p) basis set to see if it is possible to get closer to the real world results.

SUPPLEMENTAL MATERIAL

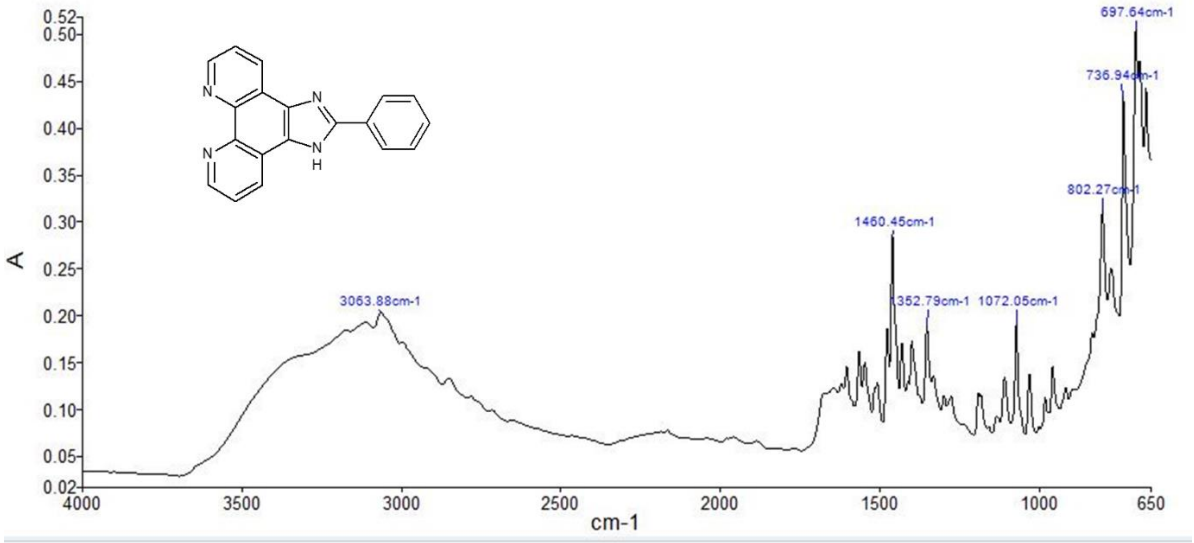

Figure 31. IR of PIP

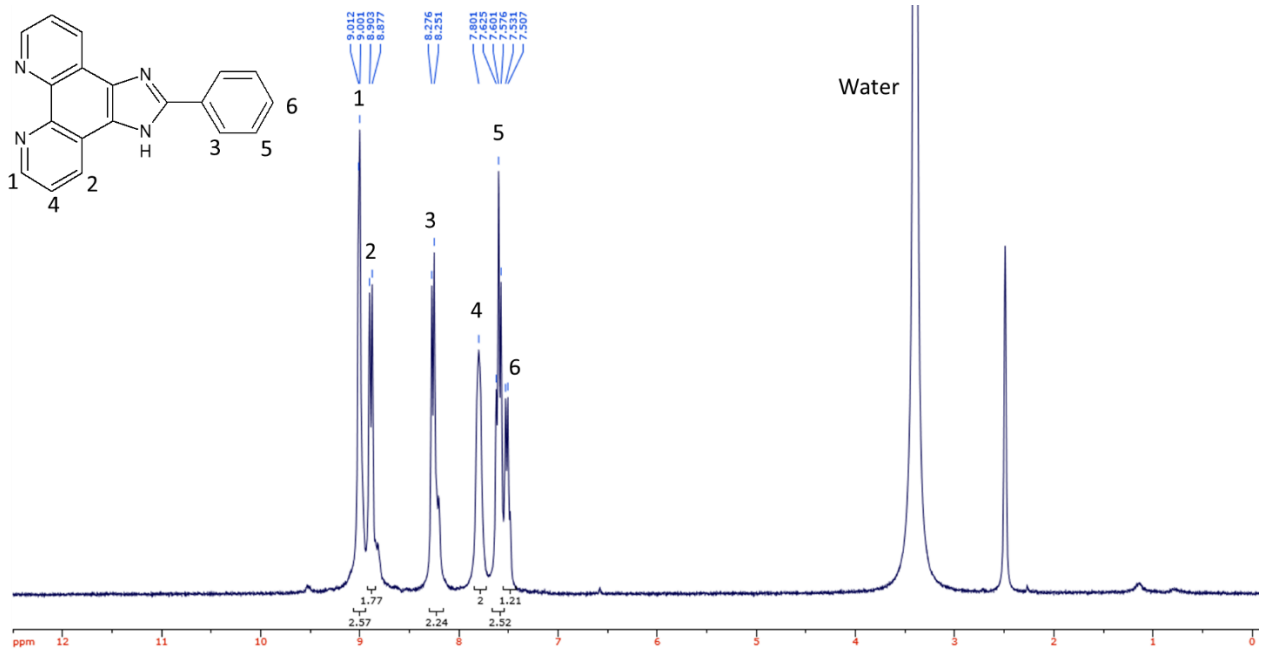

Figure 32.[1]H NMR of PIP

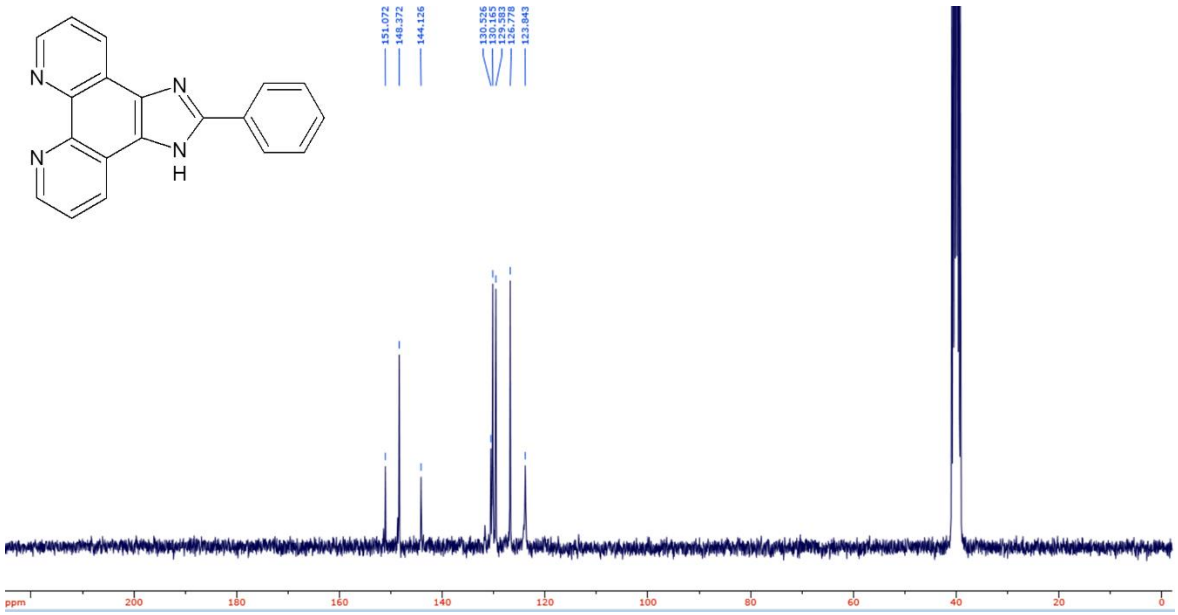

Figure 33. ^{13}C NMR of PIP

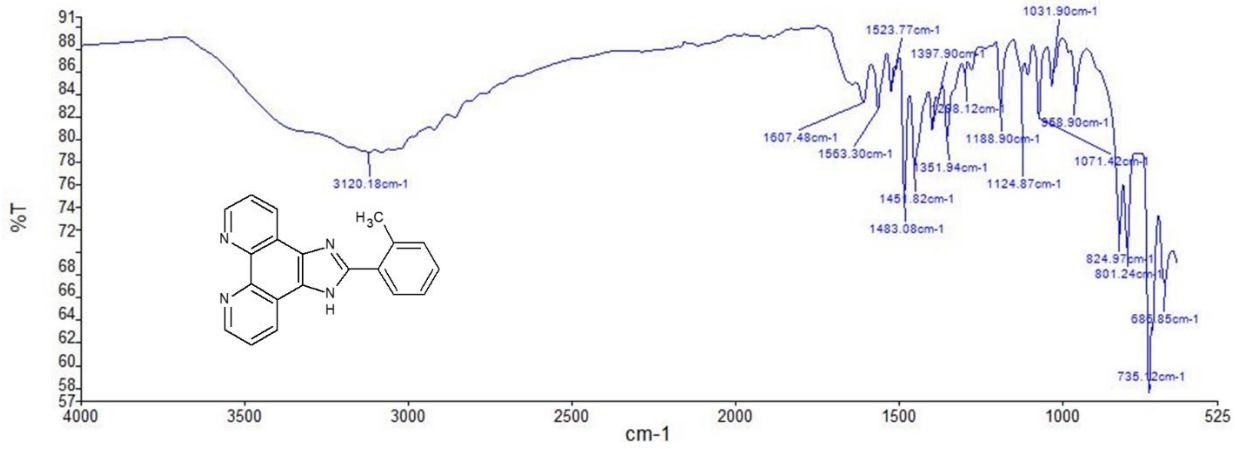

Figure 34. IR of PIP-2tolu

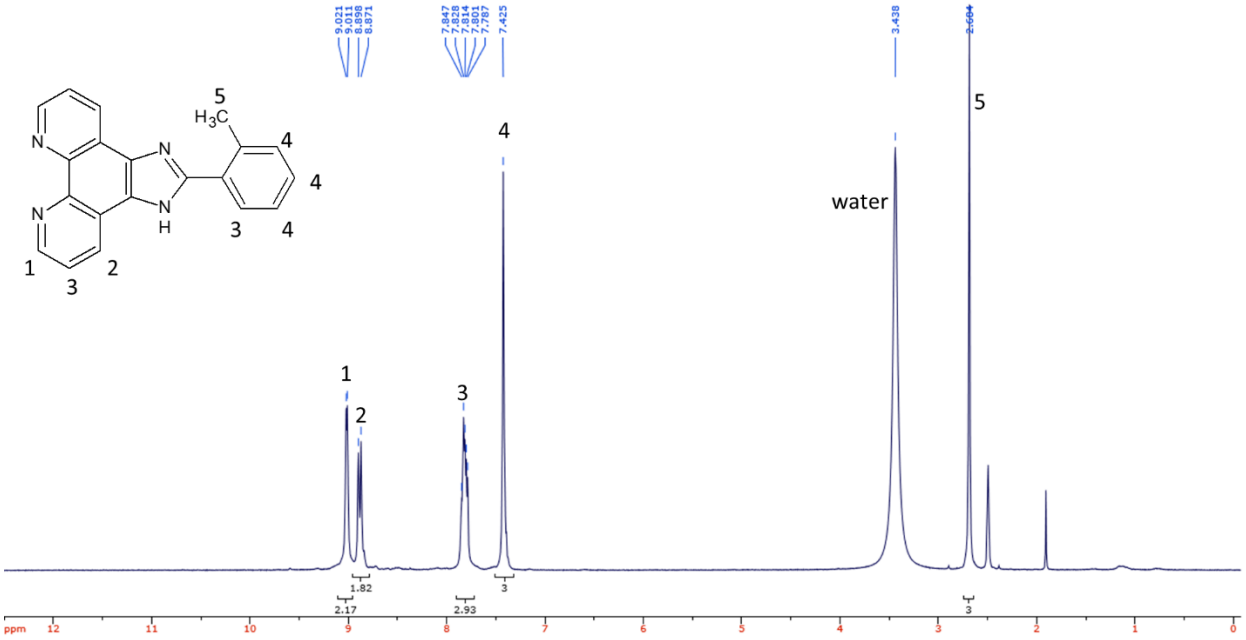

Figure 35. ^{1}H NMR of PIP-2tolu

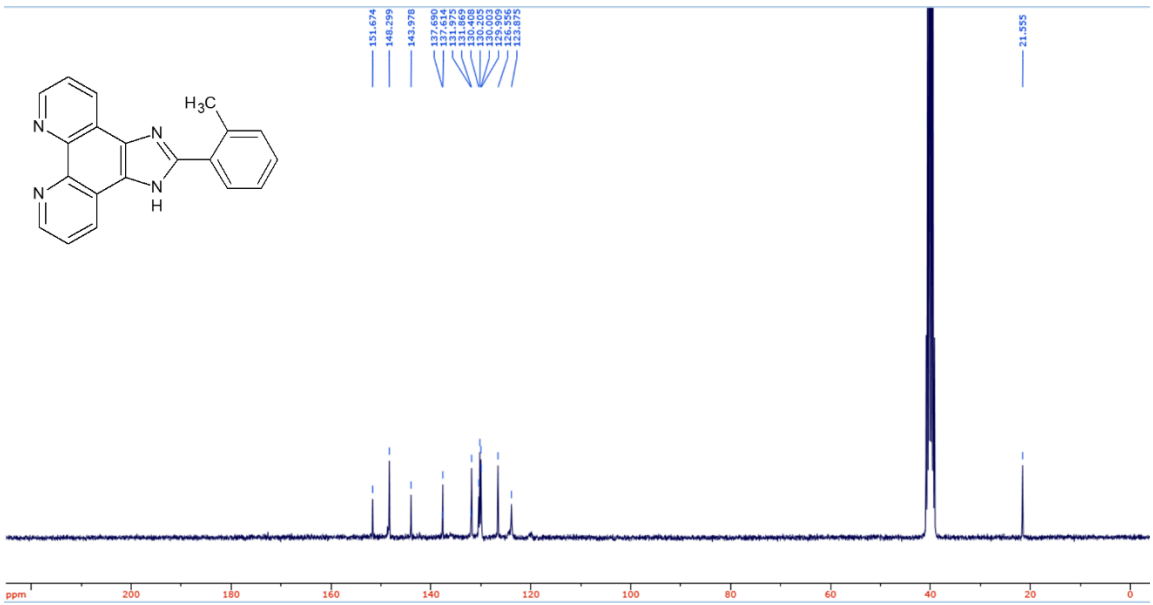

Figure 36. ^{13}C NMR or PIP-2tolu

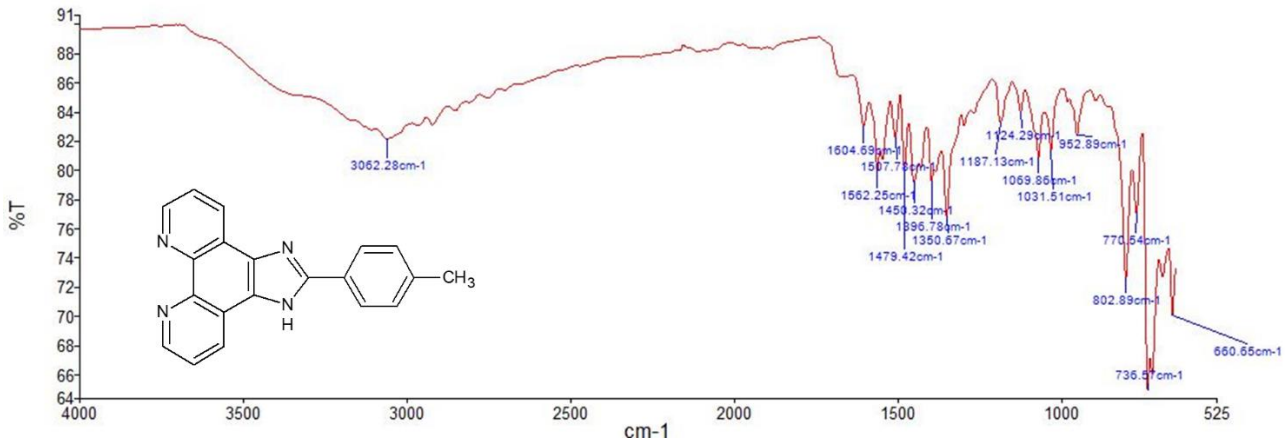

Figure 37. IR of PIP -4tolu

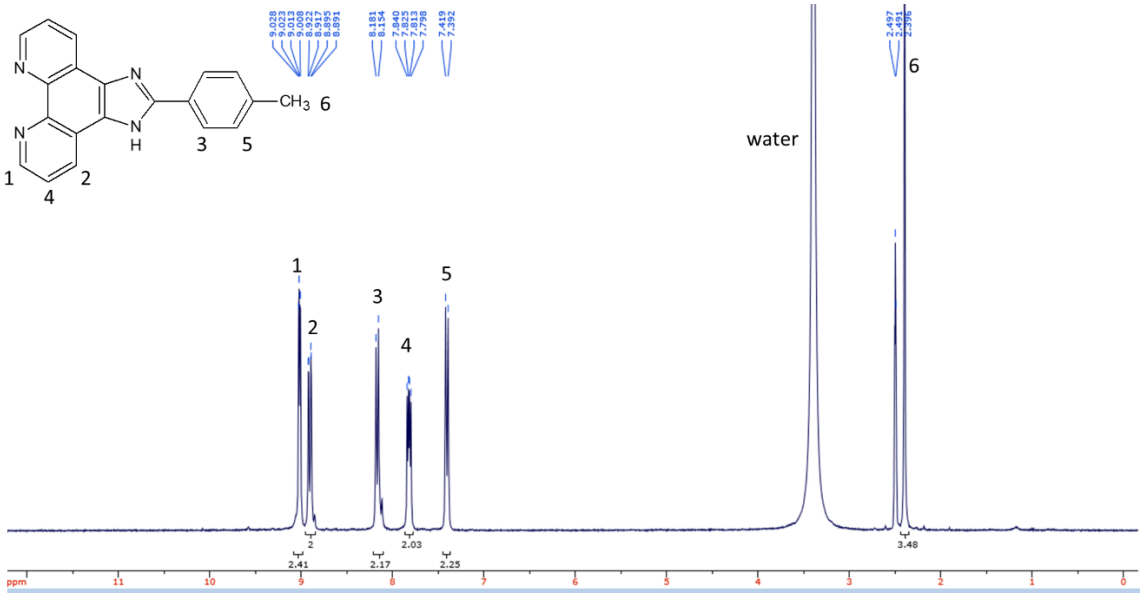

Figure 38. ^{1}H NMR of PIP-4tolu

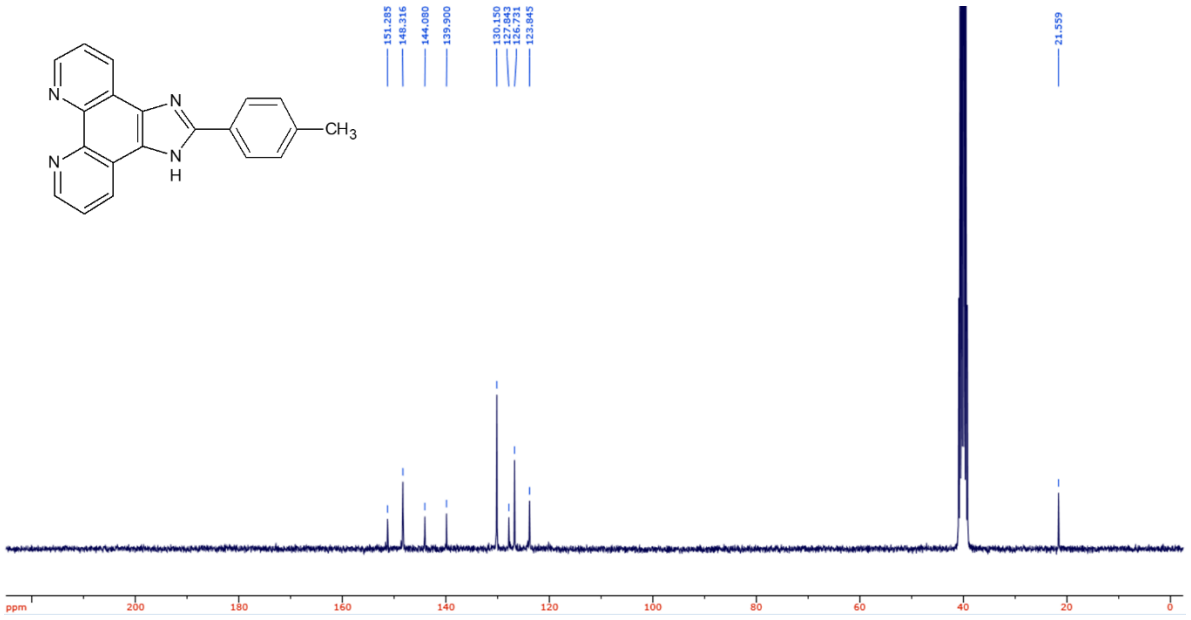

Figure 39. ^{13}C NMR of PIP-4tolu

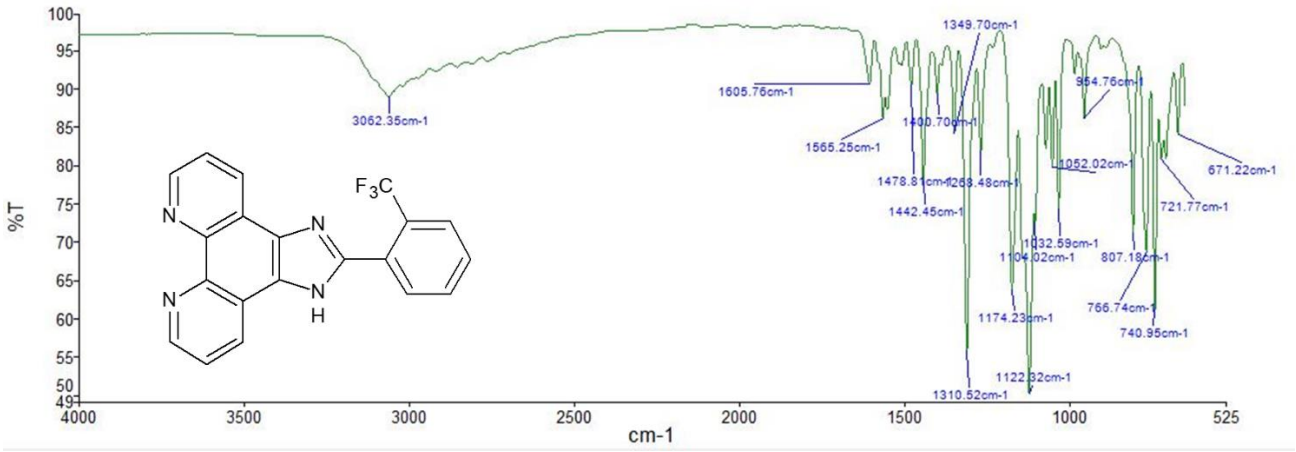

Figure 40. IR of PIP-2CF_3

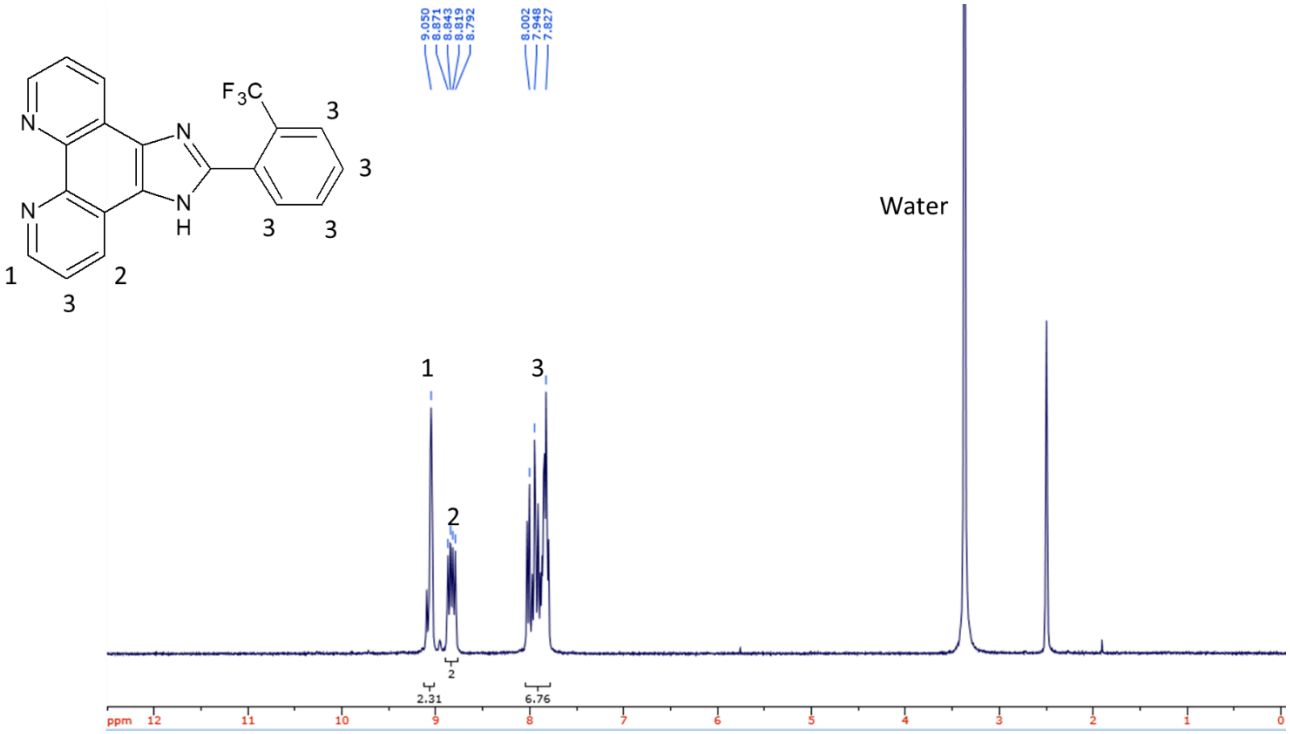

Figure 41.[1]H NMR of PIP-2CF_3

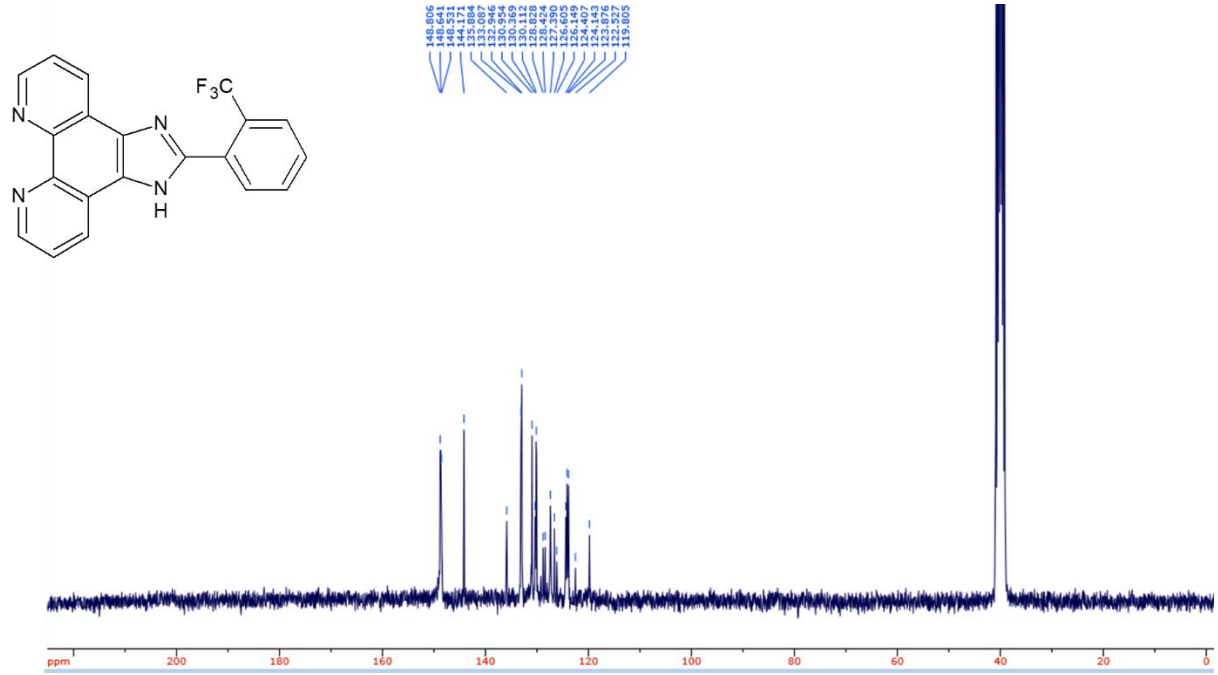

Figure 42. 13C NMR of PIP-2CF3

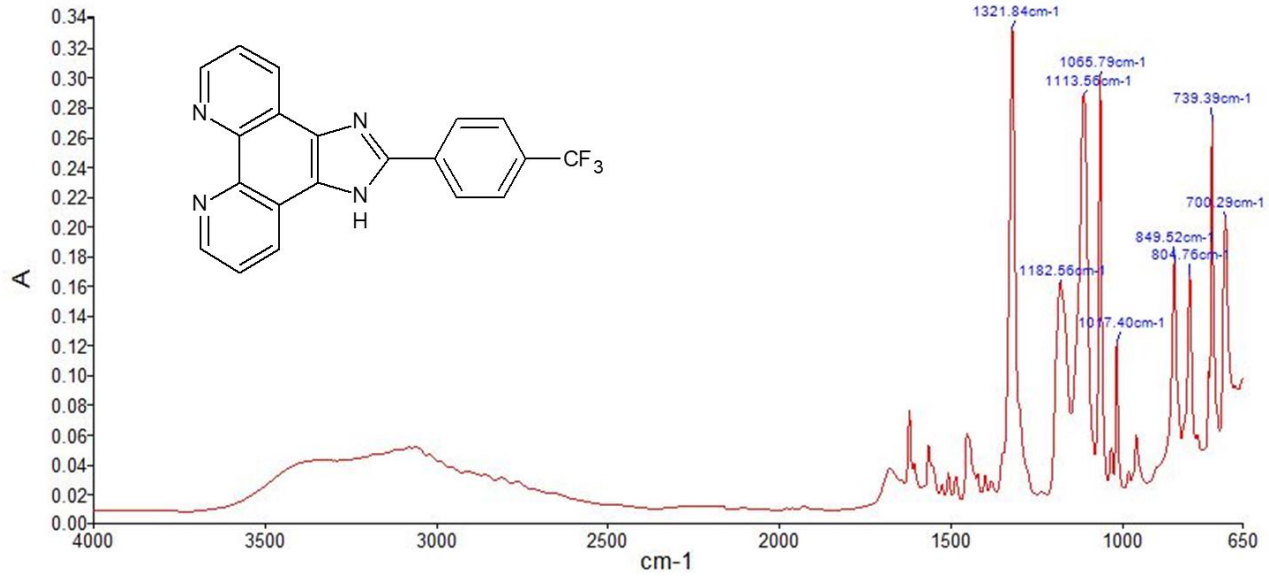

Figure 43. IR of PIP-4CF_3

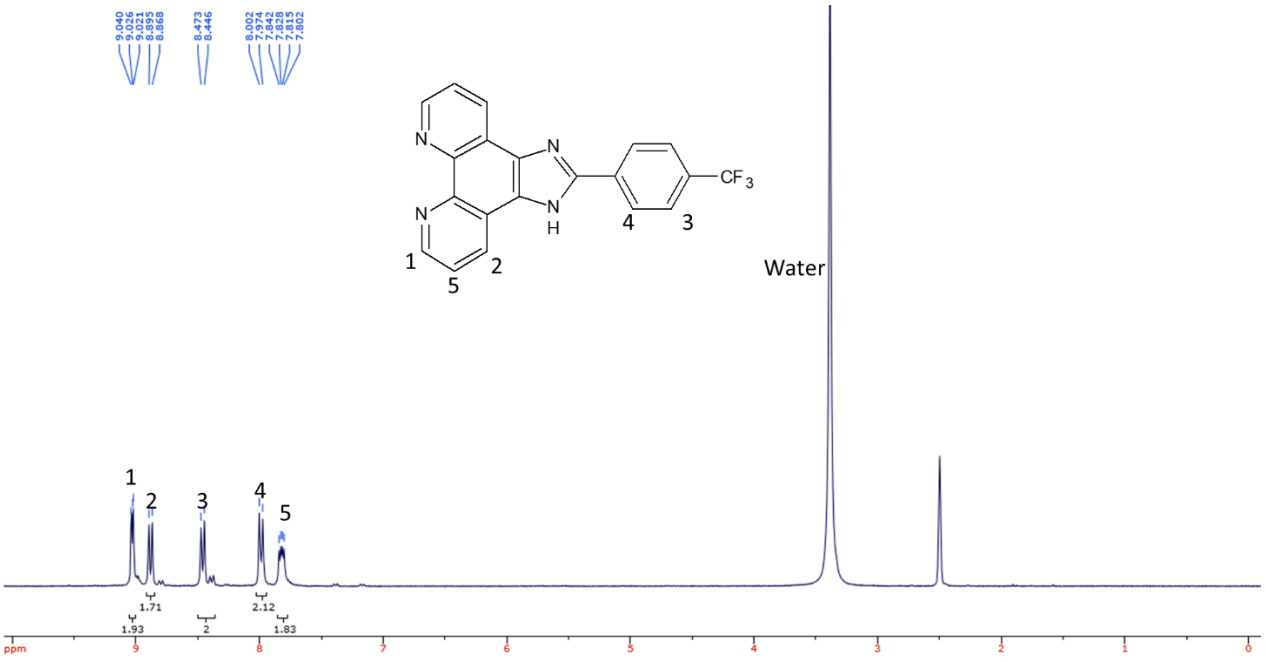

Figure 44. ^{1}H NMR of PIP-4CF_3

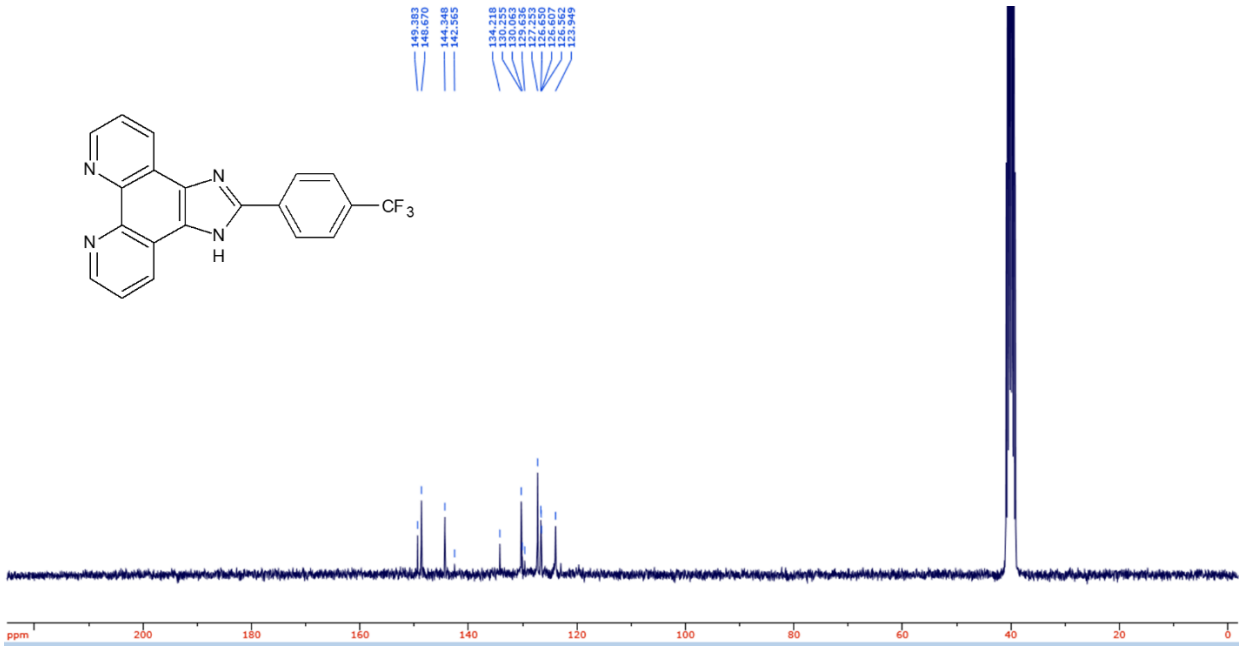

Figure 45. ^{13}C NMR of PIP-4CF_3

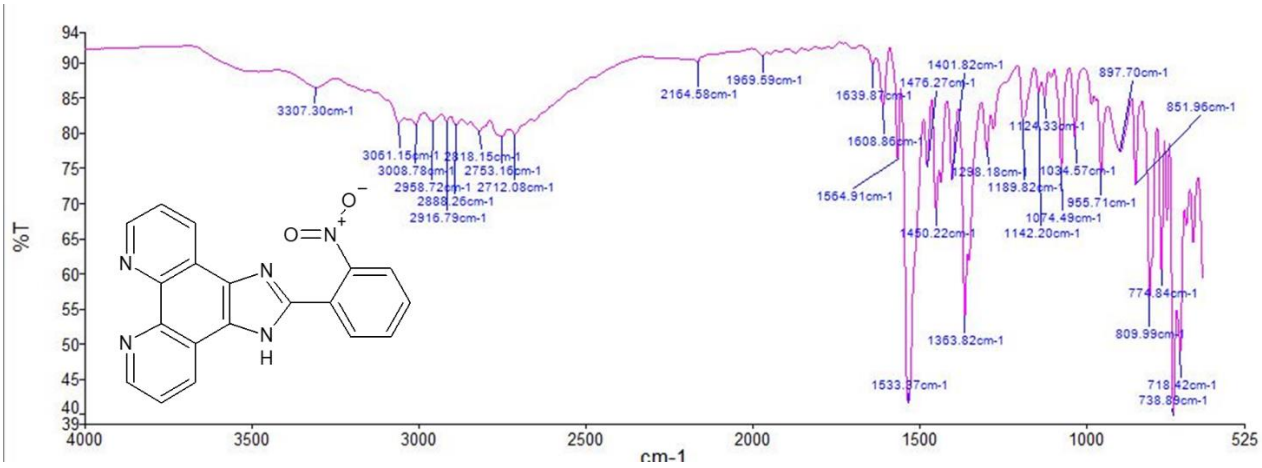

Figure 46. IR for PIP-2nitro

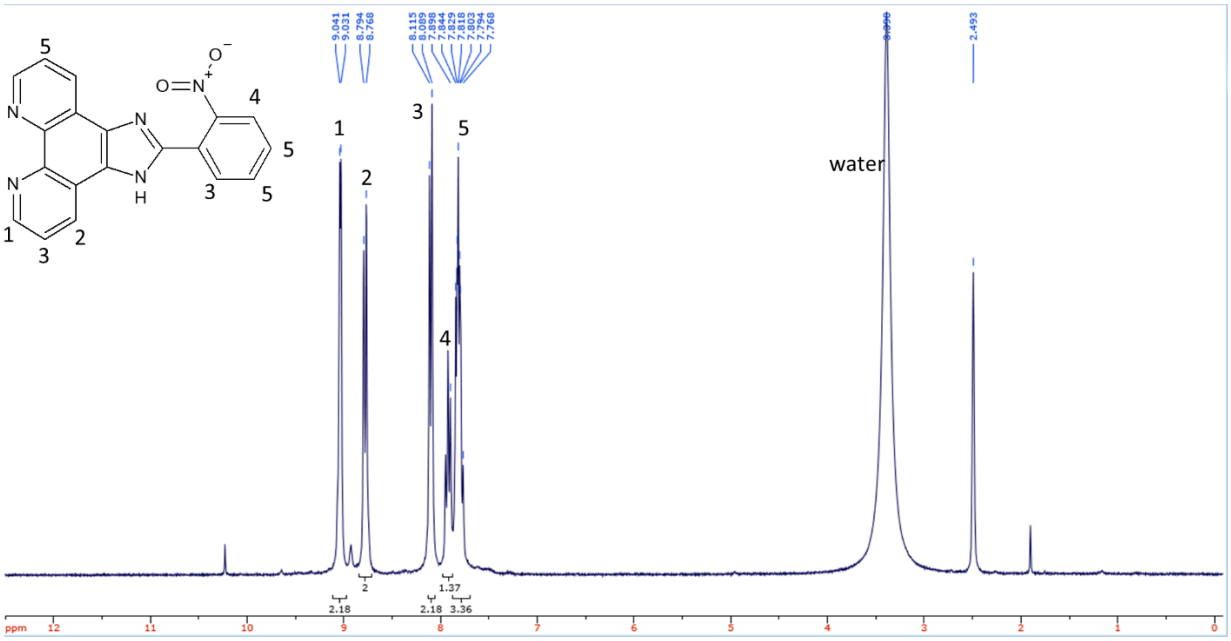

Figure 47. ^{1}H NMR for PIP-2nitro

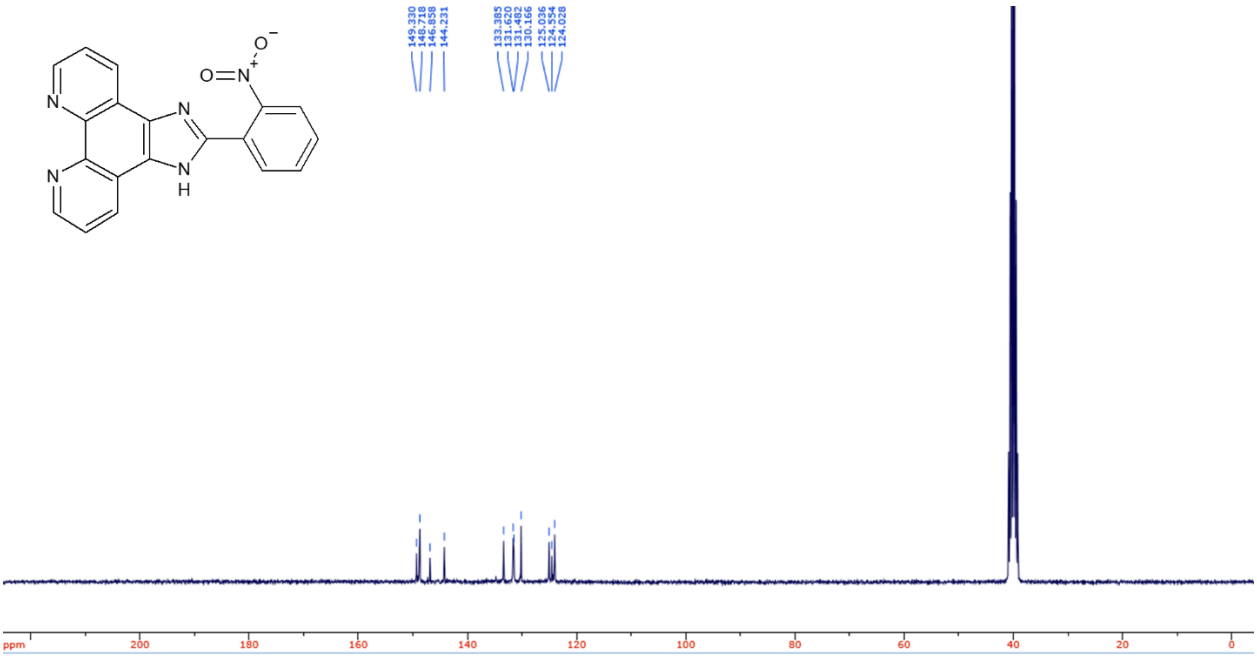

Figure 48. ^{13}C NMR for PIP-2nitro

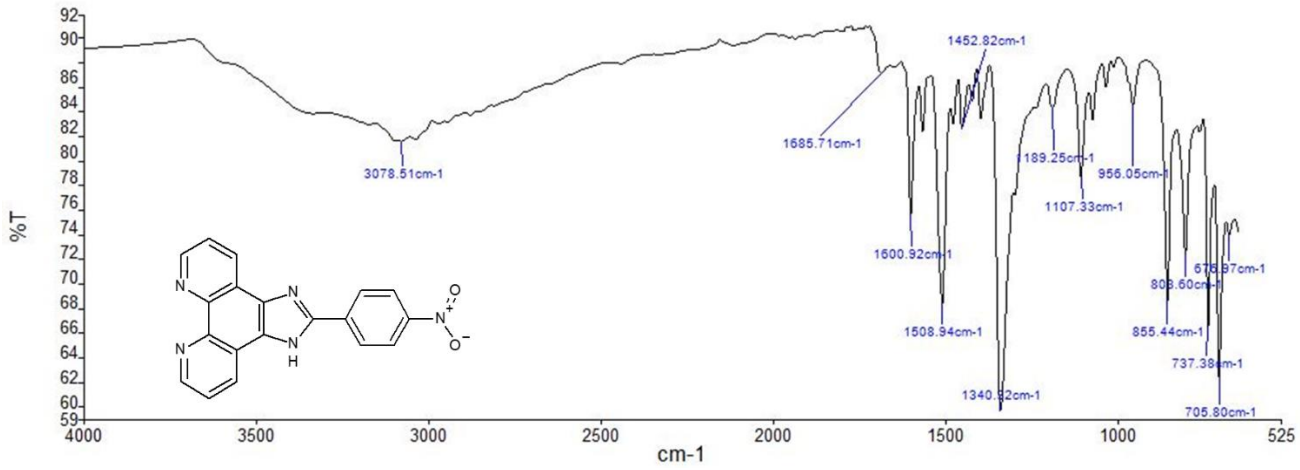

Figure 49. IR for PIP-4nitro

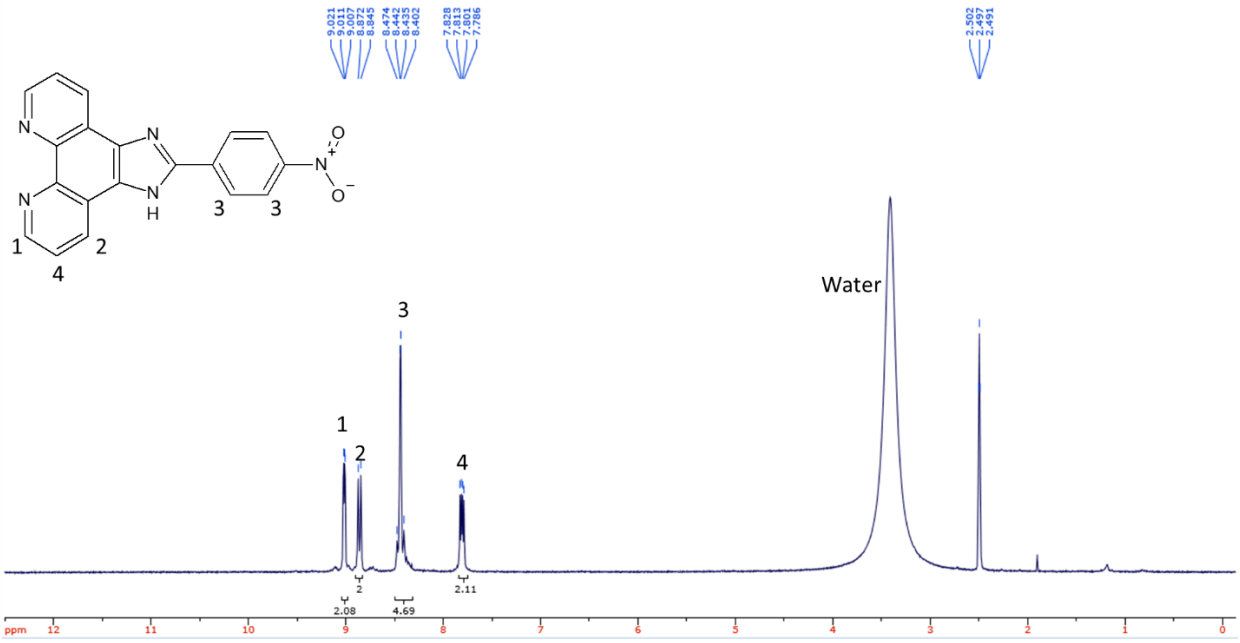

Figure 50. ^{1}H NMR for PIP-4nitro

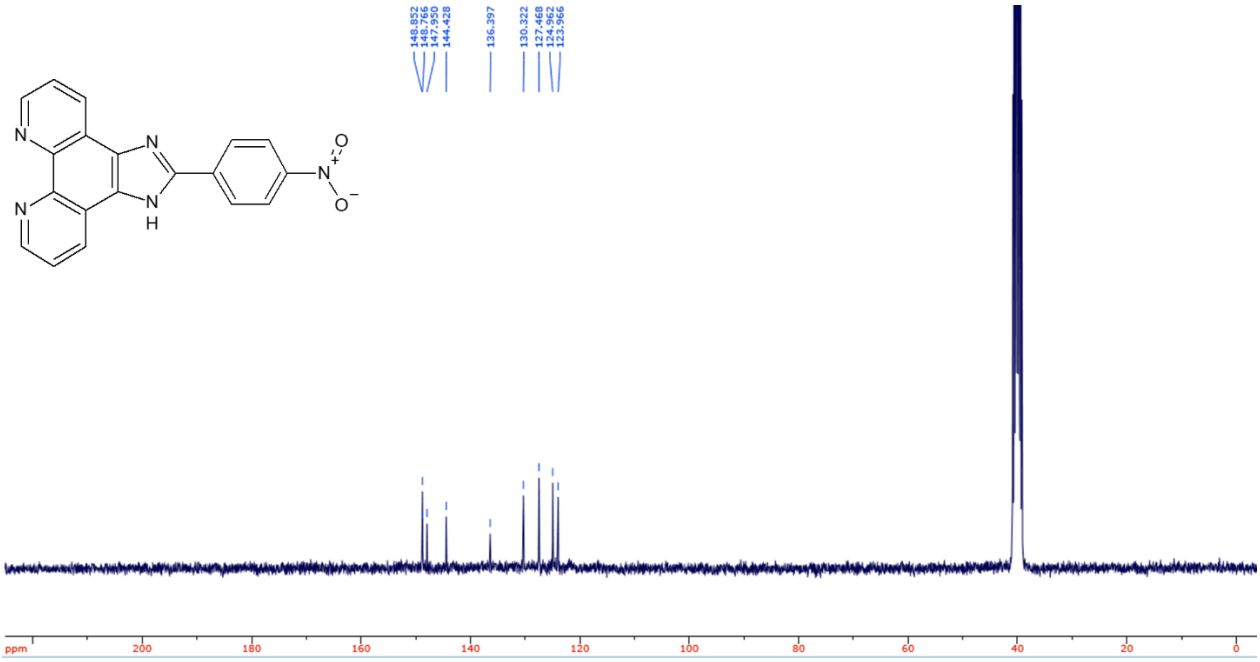

Figure 51. ^{13}C NMR for PIP-4nitro

```
%cpu=0-6
%mem=14GB
%chk=C:\Users\pventuro\Downloads\Eu-TTA-pip-4Nitro-OPT.chk
# opt b3lyp/gen geom=connectivity pseudo=read scf=maxcycle=300

Title Card Required

0 1

(XYZ coordinates of the molecule)

(Bond connectivity and order)

C N O S F H 0
6-31G*
****
Eu 0
MWB52
****

Eu 0
MWB52
```

Figure 52. Example of Gaussian Optimization input

```
Excitation energies and oscillator strengths:

Excited State   1:      Triplet-A      2.4721 eV  501.53 nm  f=0.0000  <S**2>=2.000
    247 -> 253       -0.27794
    247 -> 254        0.30371
    248 -> 254        0.15554
    249 -> 251        0.32826
    249 -> 252        0.14557
    249 -> 253        0.37007
This state for optimization and/or second-order correction.
Total Energy, E(TD-HF/TD-KS) =  -4452.04595195
Copying the excited state density for this state as the 1-particle RhoCI density.

Excited State   2:      Triplet-A      2.4761 eV  500.72 nm  f=0.0000  <S**2>=2.000
    246 -> 253       -0.10880
    247 -> 251        0.10664
    247 -> 252        0.12318
    247 -> 253       -0.14304
    247 -> 254       -0.10831
    248 -> 251       -0.30417
    248 -> 252       -0.31985
    248 -> 253        0.36750
    248 -> 254        0.15163
    249 -> 253       -0.13126

Excited State   3:      Triplet-A      2.4858 eV  498.77 nm  f=0.0000  <S**2>=2.000
```

Figure 53. Example TDDFT output file

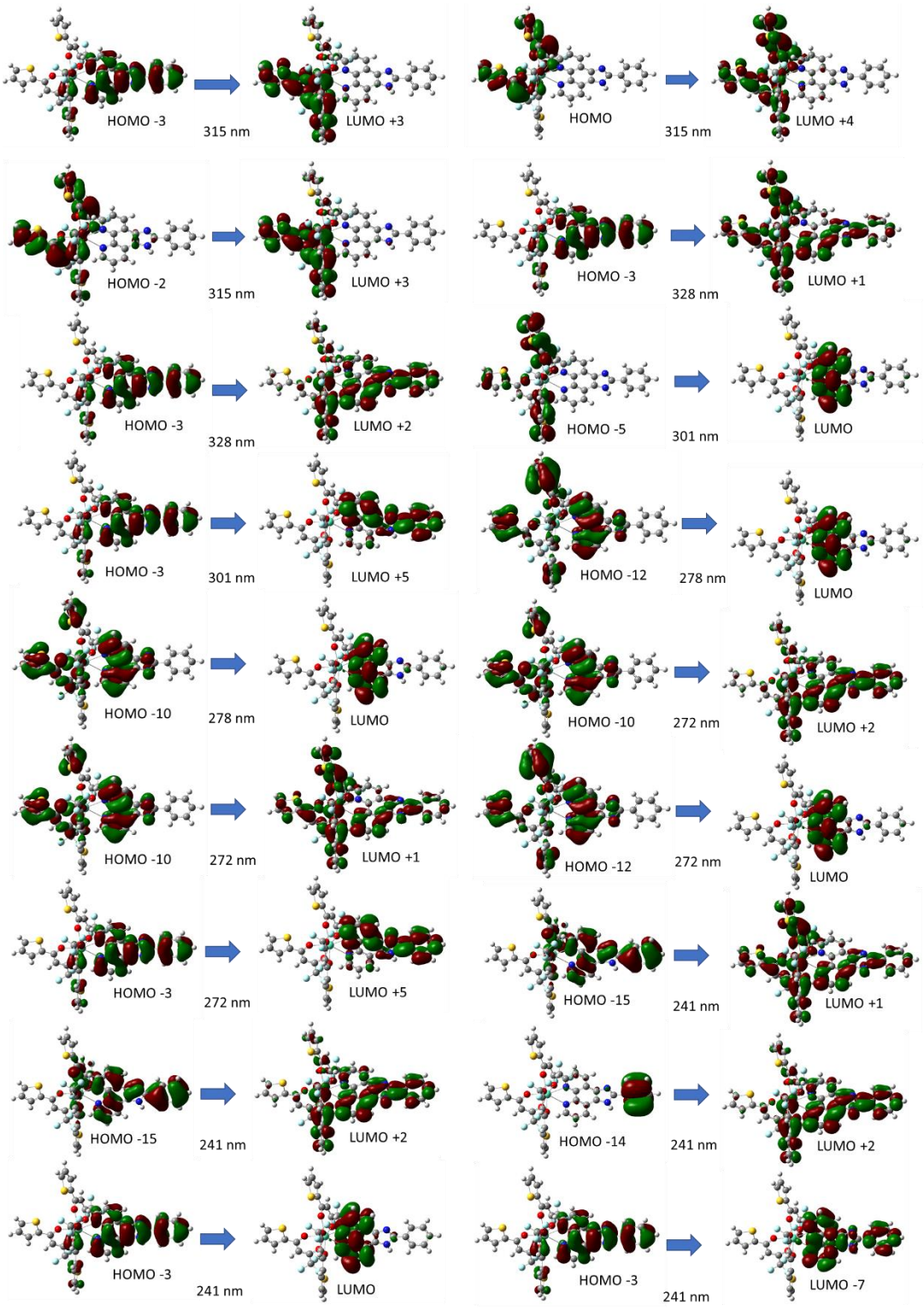

Figure 54. All orbitals responsible for the theoretical λ_{max} absorptions of $Eu(TTA)_3PIP$

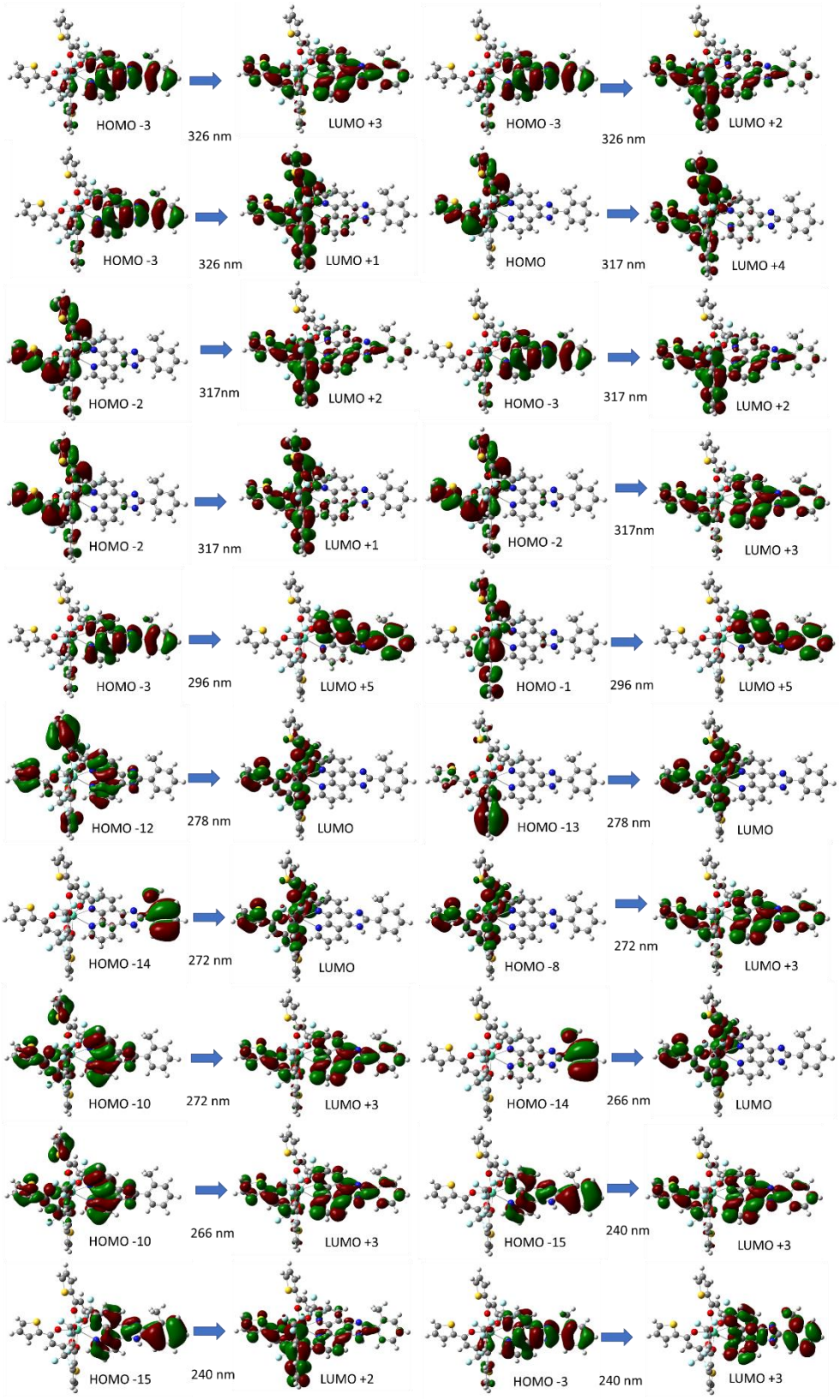

Figure 55. All orbitals responsible for the theoretical λ_{max} absorptions of $Eu(TTA)_3PIP\text{-}2tolu$

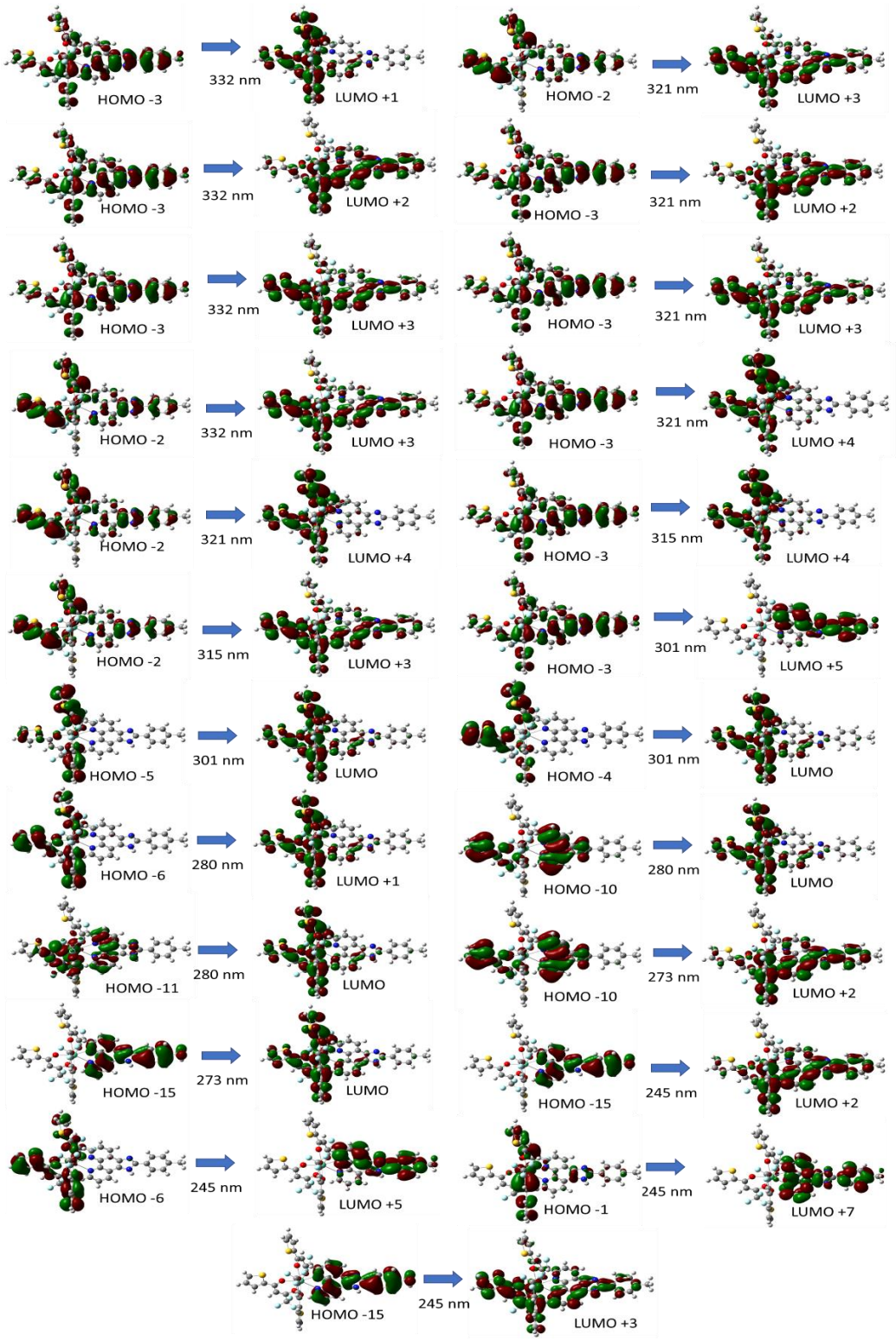

Figure 56. All orbitals responsible for the theoretical λ_{max} absorptions of $Eu(TTA)_3PIP$-4tolu

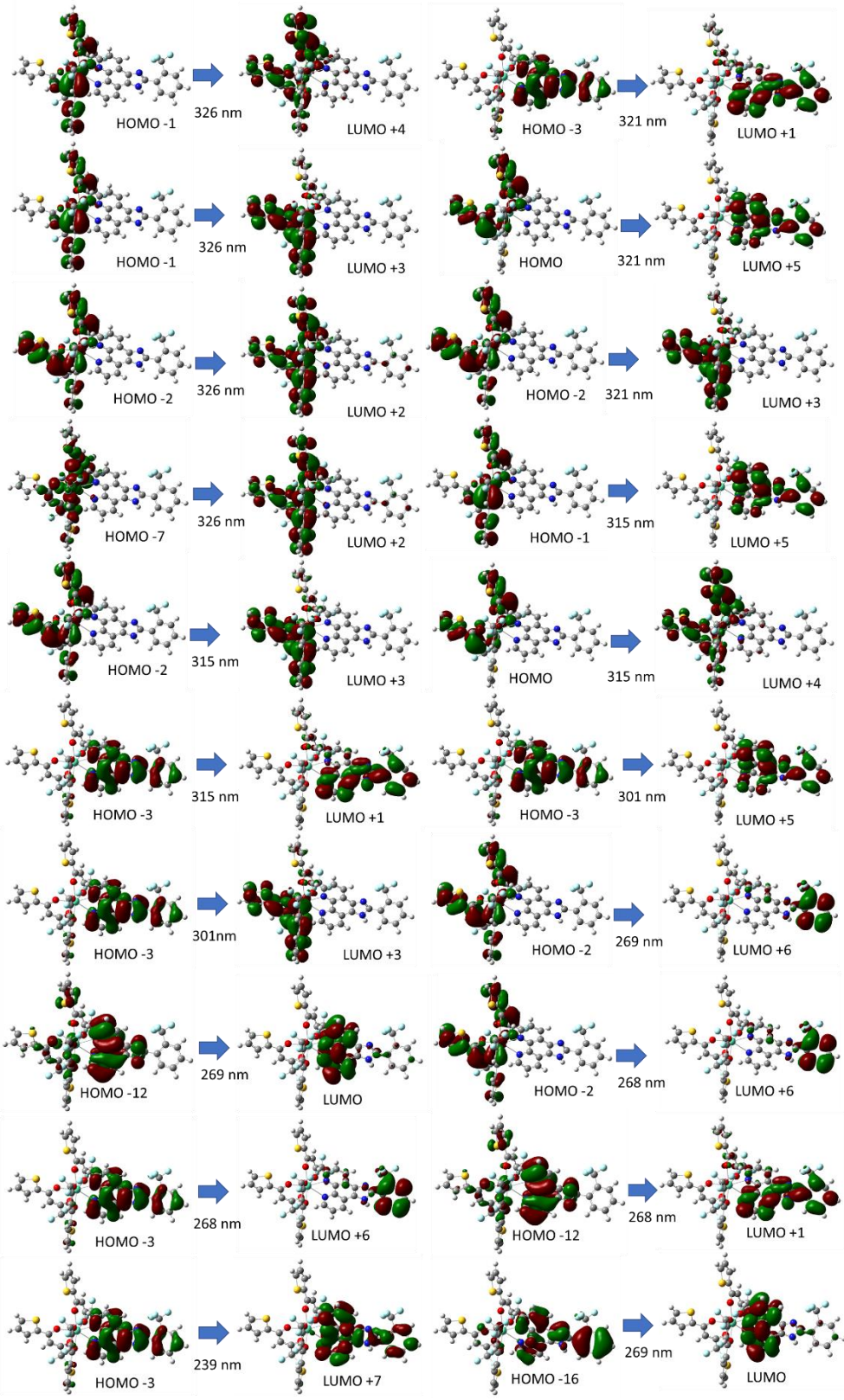

Figure 57. All orbitals responsible for the theoretical λ_{max} absorptions of $Eu(TTA)_3PIP\text{-}2CF_3$

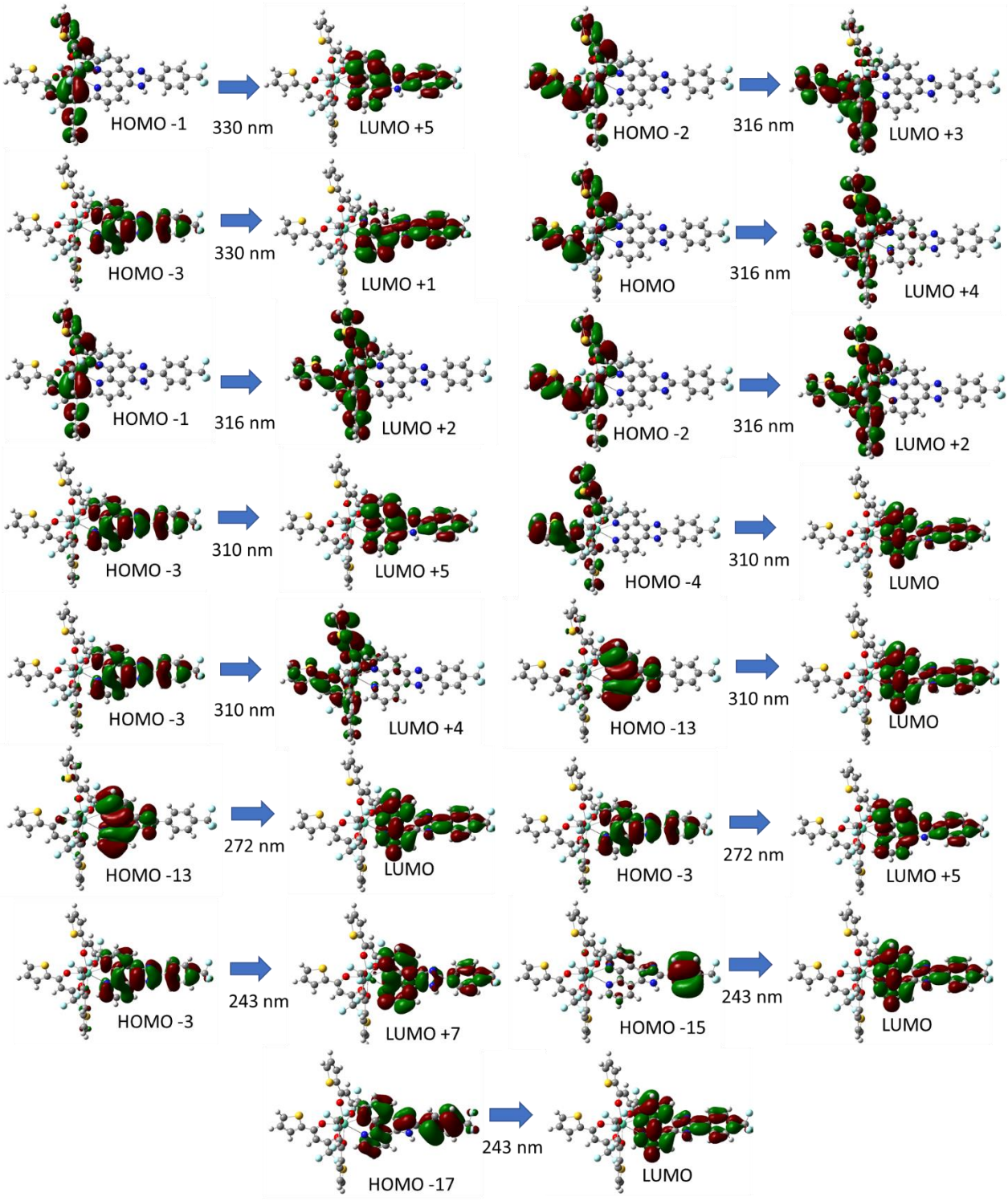

Figure 58. All orbitals responsible for the theoretical λ_{max} absorptions of $Eu(TTA)_3PIP\text{-}4CF_3$

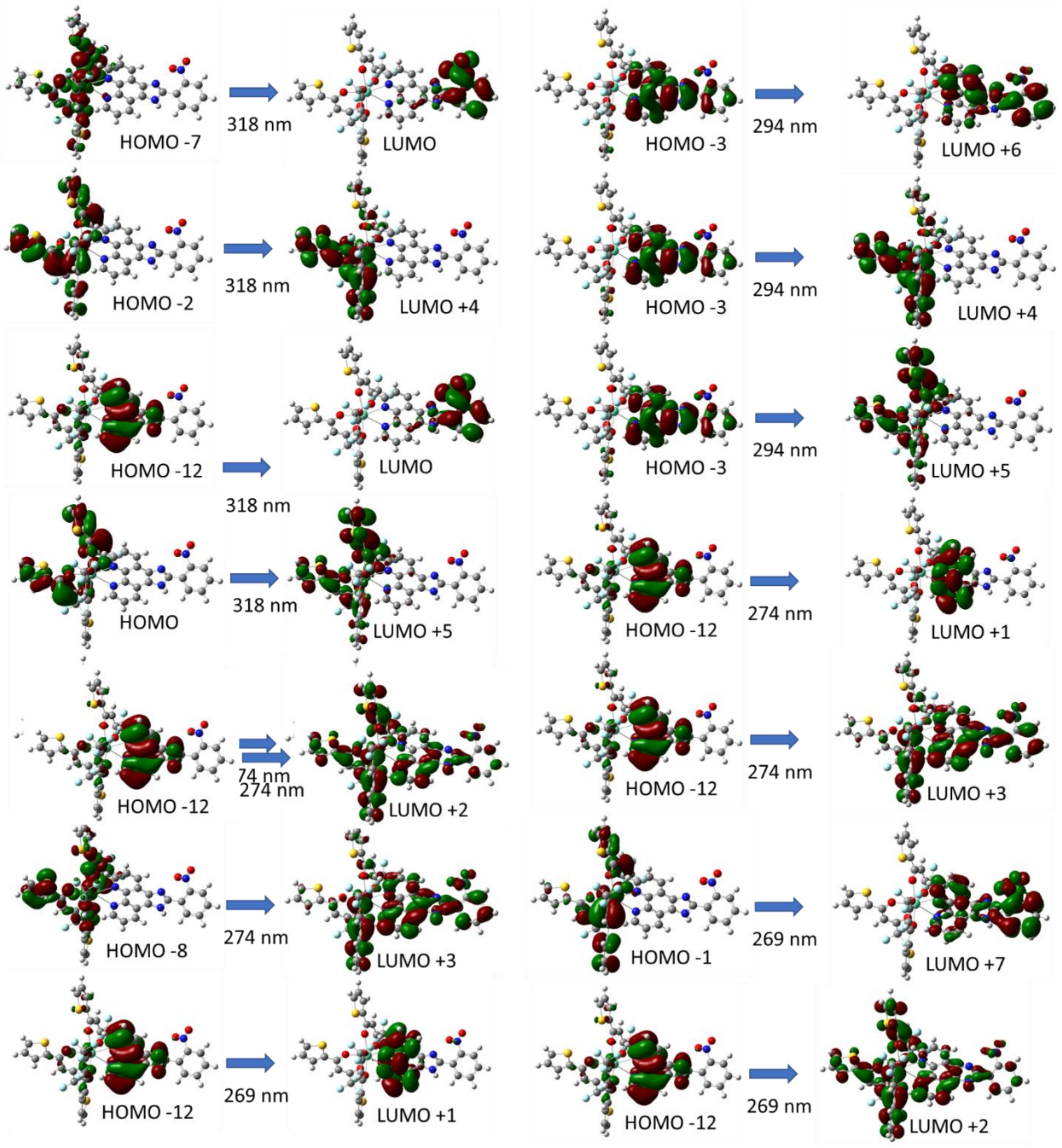

Figure 59. All orbitals responsible for the theoretical λ_{max} absorptions of $Eu(TTA)_3PIP\text{-}2NO_2$

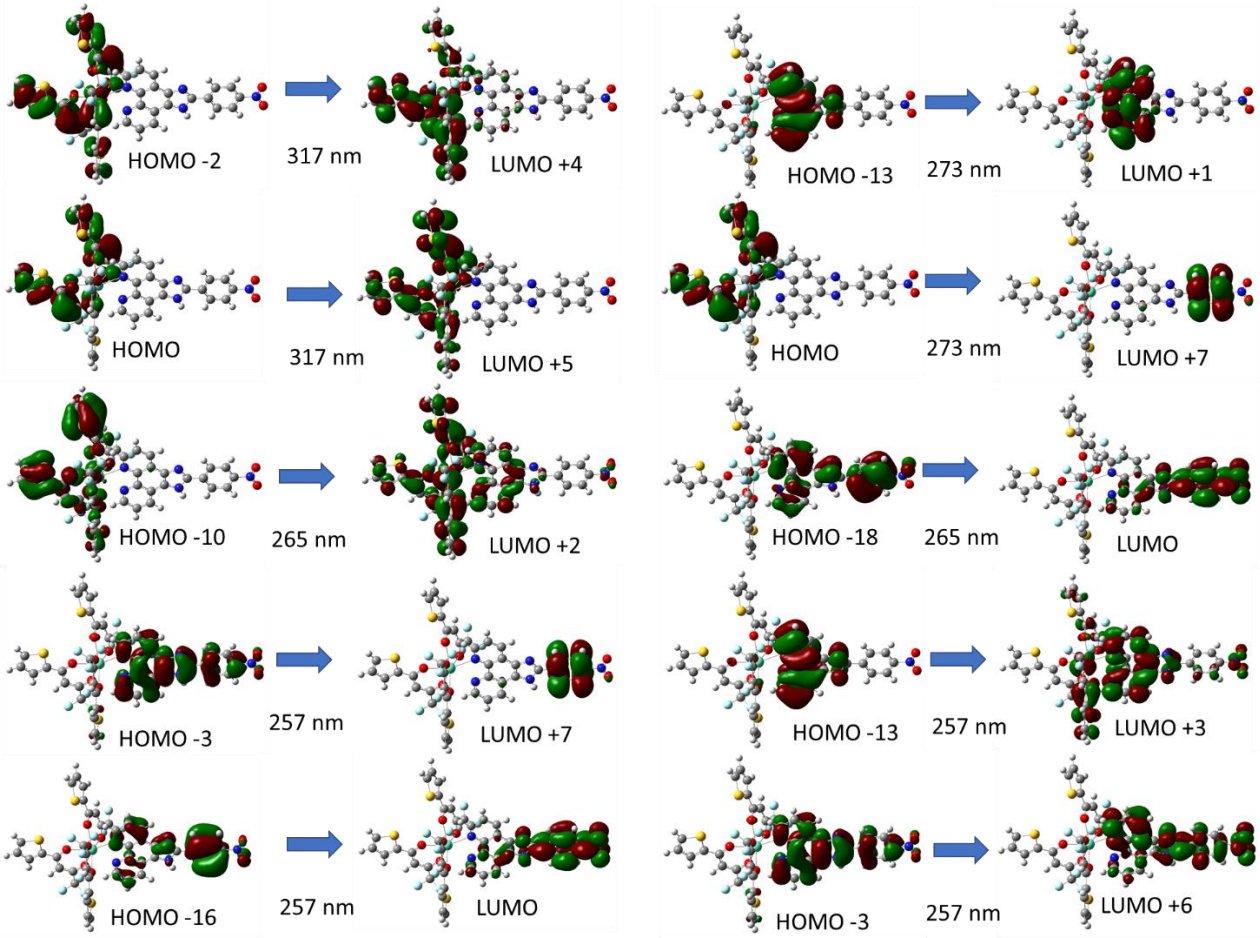

Figure 60. All orbitals responsible for the theoretical λ_{max} absorptions of $Eu(TTA)_3PIP\text{-}4NO_2$

REFERENCES

(1) Ma, Y.; Wang, Y. Recent Advances in the Sensitized Luminescence of Organic Europium Complexes. *Coord. Chem. Rev.* **2010**, *254* (9–10), 972–990.

(2) Alexandropoulos, D. I.; Cunha-Silva, L.; Pham, L.; Bekiari, V.; Christou, G.; Stamatatos, T. C. Tetranuclear Lanthanide(III) Complexes with a Zigzag Topology from the Use of Pyridine-2,6-Dimethanol: Synthetic, Structural, Spectroscopic, Magnetic and Photoluminescence Studies. *Inorg. Chem.* **2014**, *53* (6), 3220–3229.

(3) Crosby, G. A.; Whan, R. E.; Freeman, J. J. Spectroscopic Studies of Rare Earth Chelates. *J. Phys. Chem.* **1962**, *66* (12), 2493–2499.

(4) Greco, C.; Moro, G.; Bertini, L.; Biczysko, M.; Barone, V.; Cosentino, U. Computational Investigation on the Spectroscopic Properties of Thiophene Based Europium β-Diketonate Complexes. *J. Chem. Theory Comput.* **2014**, *10* (2), 767–777.

(5) Døssing, A. Luminescence from Lanthanide(3+) Ions in Solution. *Eur. J. Inorg. Chem.* **2005**, No. 8, 1425–1434.

(6) Latva, M.; Takalob, H.; Mukkala, V. M.; Matachescu, C.; Rodríguez-Ubis, J. C.; Kankare, J. Correlation between the Lowest Triplet State Energy Level of the Ligand and Lanthanide(III) Luminescence Quantum Yield. *J. Lumin.* **1997**, *75* (2), 149–169.

(7) De Silva, C. R.; Li, J.; Zheng, Z.; Corrales, L. R. Correlation of Calculated Excited-State Energies and Experimental Quantum Yields of Luminescent Tb(III) β-Diketonates. *J. Phys. Chem. A* **2008**, *112* (20), 4527–4530.

(8) Chizhik, A. I.; Gregor, I.; Enderlein, J. Quantum Yield Measurement in a Multicolor Chromophore Solution Using a Nanocavity. *Nano Lett.* **2013**, *13* (3), 1348–1351.

(9) Armelao, L.; Quici, S.; Barigelletti, F.; Accorsi, G.; Bottaro, G.; Cavazzini, M.; Tondello, E. Design of Luminescent Lanthanide Complexes: From Molecules to Highly Efficient Photo-Emitting Materials. *Coord. Chem. Rev.* **2010**, *254* (5–6), 487–505.

(10) De Bettencourt-Dias, A. Lanthanide-Based Emitting Materials in Light-Emitting Diodes. *J. Chem. Soc. Dalt. Trans.* **2007**, No. 22, 2229–2241.

(11) Shahi, P. K.; Singh, A. K.; Singh, S. K.; Rai, S. B.; Ullrich, B. Revelation of the Technological Versatility of the Eu(TTA)3Phen Complex by Demonstrating Energy Harvesting, Ultraviolet Light Detection, Temperature Sensing, and Laser Applications. *ACS Appl. Mater. Interfaces* **2015**, *7* (33), 18231–18239.

(12) Yu, Z.; Guo, J.; Li, D.; Lin, H. Polyvinylpyrrolidone for Enhanced Solar Cell. *Hindawi* **2019**, *2019*.

(13) Singh, K.; Boddula, R.; Vaidyanathan, S. Versatile Luminescent Europium(III)-β-Diketonate-Imidazo-Bipyridyl Complexes Intended for White LEDs: A Detailed Photophysical and Theoretical Study. *Inorg. Chem.* **2017**, *56* (15), 9376–9390.

(14) Kumar, S.; Maji, S.; Ramanathan, N.; Sundararajan, K. Complexation of Eu(III) with Furan Monocarboxylates in Aqueous Medium at Variable Temperatures: Luminescence and Computational Studies. *J. Lumin.* **2019**, *212* (March), 83–91.

(15) Taha, Z. A.; Ajlouni, A. M.; Ababneh, T. S.; Al-Momani, W.; Hijazi, A. K.; Al Masri, M.; Hammad, H. DFT Computational Studies, Biological and Antioxidant Activities, and

Kinetic of Thermal Decomposition of 1,10-Phenanthroline Lanthanide Complexes. *Struct. Chem.* **2017**, *28* (6), 1907–1918.

(16) Lewars, E. G. *Computational Chemistry*; Springer, Dordrecht, 2016.

(17) Young, D. *Computational Chemistry: A Practical Guide for Applying Techniques to Real World Problems*, 1st ed.; Wiley-Interscience: Hoboken, NJ, 2001; Vol. 9.

(18) Cai, Z.; Zhou, M.; Xu, J. Degenerate Four-Wave Mixing Determination of Third-Order Optical Nonlinearities of Three Mixed Ligand Nickel(II) Complexes. *J. Mol. Struct.* **2011**.

(19) Leonard, J. P.; Gunnlaugsson, T. Luminescent Eu(III) and Tb(III) Complexes: Developing Lanthanide Luminescent-Based Devices. *J. Fluoresc.* **2005**, *15* (4), 585–595.

(20) Frediani, A. M. SYNTHESIS OF TIME-RESOLVED FLUORESCENCE PROBES FOR THE FUTURE DETECTION AND IMPROVED STUDY OF CANCER. 2019.

(21) Damavandi, S.; Sandaroos, R. L-Proline-Catalyzed Three-Component Synthesis of Condensed Imidazoles. *Arab. J. Chem.* **2016**, *9*, S1138–S1143.

(22) Zheng, Y.; Zhou, Y.; Yu, J.; Yu, Y.; Zhang, H.; Gillin, W. P. Electroluminescence from 5D0 → 7FJ and 5D1 → 7FJ (J = 0-4) Transitions with a Europium Complex as Emitter. *J. Phys. D. Appl. Phys.* **2004**, *37* (4), 531–534.